

Origins of the Loss of Concertedness in Pericyclic Reactions: Theoretical Prediction and Direct Observation of Stepwise Mechanisms in [3 + 2] Thermal Cycloadditions

Silvia Vivanco,[†] Begoña Lecea,[‡] Ana Arrieta,[†] Pilar Prieto,[§] Iñaki Morao,[†] Anthony Linden,^{||} and Fernando P. Cossío^{*,†}

Contribution from the Kimika Fakultatea, Euskal Herriko Unibertsitatea, P.K. 1072, 20080, San Sebastián-Donostia, Spain, Farmazi Fakultatea, Euskal Herriko Unibertsitatea, P.K. 450, 01080 Vitoria-Gasteiz, Spain, Facultad de Química, Universidad de Castilla-la Mancha, 13071 Ciudad Real, Spain, and Organisch-chemisches Institut der Universität Zürich, Winterthurststrasse 190, CH-8057, Zürich, Switzerland

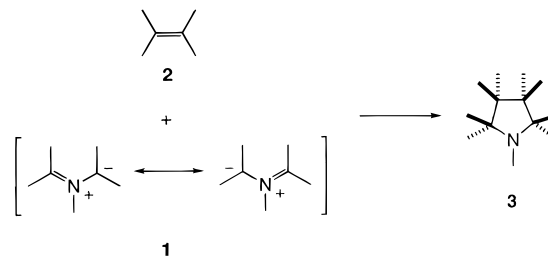
Received December 30, 1999

Abstract: Several [3 + 2] thermal cycloadditions between azomethine ylides and nitroalkenes have been studied both theoretically and experimentally. When the N-metalated 1,3-dipoles are used, the reaction is stepwise. The corresponding zwitterionic intermediates have been located computationally and observed by NMR monitoring. In the case of N-unsubstituted azomethine ylides, the reaction can be concerted or stepwise, depending upon the ability of the substituents to stabilize zwitterionic intermediates. A general model is proposed to explain the observed phenomena. This simple model can be extended to other thermal cycloadditions to predict the stepwise or concerted nature of their mechanisms without computing complete reaction coordinates.

Introduction

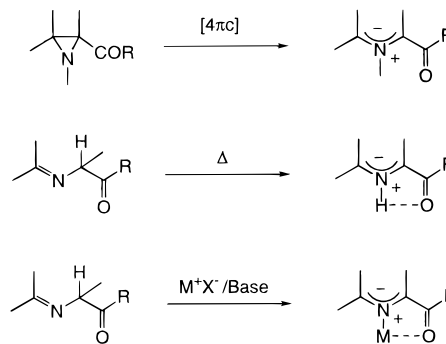
The [3 + 2] cycloadditions constitute one of the most efficient and general methods for the synthesis of five-membered rings.¹ Among the different versions of the reaction developed over the years, the [3 + 2] cycloadditions between azomethine ylides **1** and olefins **2** (Scheme 1) provide ready convergent access to pyrrolidine² nuclei **3**, whose importance in medicinal and synthetic organic chemistry is well-known. This reaction is particularly efficient when the azomethine ylide is stabilized by a carbonyl group. In this case, the corresponding [3 + 2] cycloaddition leads to highly substituted proline derivatives. There are at least three general methods for the generation of these azomethine ylides (Scheme 2). The first one consists of the conrotatory ring opening of conveniently substituted aziridines. This method was used by Huisgen³ to perform his seminal

Scheme 1^a



^a In this and other schemes, unless otherwise stated, the possible substituents at the different positions are not specified.

Scheme 2



studies on the mechanism of the generation of 1,3-dipoles and their subsequent cycloaddition reactions with alkenes. The second method⁴ consists of the isomerization of an imine derivative of an α -aminoester containing an enolizable hydrogen to yield the azomethine ylide which can be trapped by reaction

[†] Kimika Fakultatea.

[‡] Farmazi Fakultatea.

[§] Facultad de Química.

^{||} Organisch-chemisches Institut.

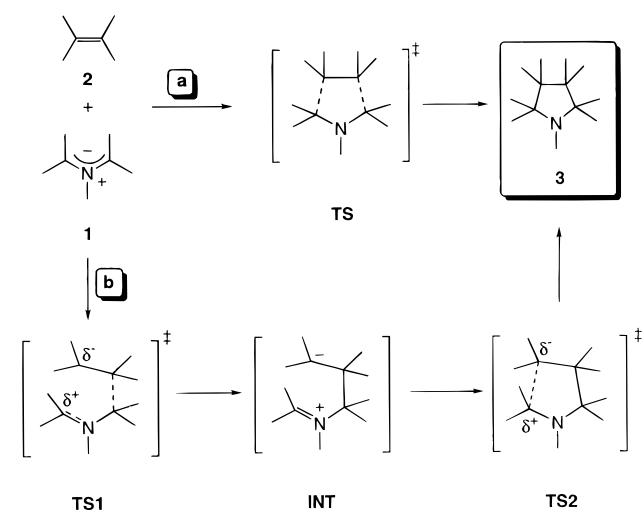
(1) (a) Huisgen, R. *Angew. Chem., Int. Ed. Engl.* **1963**, *2*, 565. (b) *1,3-Dipolar Cycloaddition Chemistry*; Padwa, A., Ed.; Wiley: New York, 1984; Vols. 1–2. (c) Cinquini, M.; Cozzi, F. In *Stereoselective Synthesis*; Helmchen, G.; Hoffmann, R. W.; Mulzer, J.; Schauman, E., Eds.; Georg Thieme: Stuttgart 1996; Vol. 5, pp 2953–2987. (d) Padwa, A. In *Comprehensive Organic Synthesis*; Trost, B. M.; Fleming, I., Eds.; Pergamon: Oxford, 1991; Vol. 4, pp 1069–1109. (e) Wade, P. A. In *Comprehensive Organic Synthesis*; Trost, B. M.; Fleming, I., Eds.; Pergamon: Oxford, 1991; Vol. 4, pp 1111–1168.

(2) (a) Lown, J. W. In *1,3-Dipolar Cycloaddition Chemistry*; Padwa, A., Ed.; Wiley: New York, 1984; Vol. 1, pp 653–732. (b) Grigg, R. *Chem. Soc. Rev.* **1987**, *16*, 89. (c) Tsuge, O.; Kanemasa, S. In *Advances in Heterocyclic Chemistry*; Katritzky, A. R., Ed.; Academic Press: San Diego, 1989; Vol. 45, pp 232–349. (d) Vedejs, E. In *Advances in Cycloaddition*; Curran, D. P., Ed.; Jai Press: Greenwich, 1988; Vol. 1, pp 33–51.

(3) (a) Huisgen, R.; Scheer, W.; Mader, H. *Angew. Chem., Int. Ed. Engl.* **1969**, *8*, 602. (b) Huisgen, R.; Mader, H. *J. Am. Chem. Soc.* **1971**, *93*, 1777. (c) Hermann, H.; Huisgen, R.; Mader, H. *J. Am. Chem. Soc.* **1971**, *93*, 1779. (d) Huisgen, R.; Scheer, W.; Mader, H.; Brunn, E. *Angew. Chem., Int. Ed. Engl.* **1969**, *8*, 604.

(4) (a) Grigg, R.; Kemp, J. *J. Chem. Soc., Chem. Commun.* **1978**, 109. (b) Grigg, R.; Kemp, J. *Tetrahedron Lett.* **1980**, *21*, 1461. (c) Grigg, R. *Bull. Soc. Chim. Belg.* **1984**, *93*, 593.

Scheme 3



with the corresponding dipolarophile. Alternatively, the same substrate can be readily transformed into its N-metalated azomethine ylide with the appropriate salt in the presence of base.^{2c,5-7} This kind of reaction has proved to be remarkably efficient in its possible asymmetric versions.⁸ In addition, the reaction tolerates a wide range of substituents and is therefore well-suited for combinatorial synthesis.⁹

Given the importance of the reaction, the elucidation of its mechanism is crucial to understand the variables that determine its regio- and stereocontrol. After a vivid debate,^{10,11} it is now accepted that in general the reaction is concerted, according to the *supra-supra* mechanism proposed by Huisgen (Scheme 3, path a).¹² Several years later, Huisgen himself¹³ found a [3 + 2] cycloaddition whose mechanism was demonstrated to be stepwise, zwitterionic structures being the reaction intermediates. Finally, Schleyer et al.¹⁴ have recently shown that anionic [3 + 2] cycloadditions take place via stepwise mechanisms. However,

(5) Kanemasa, S.; Tsuge, O. In *Advances in Cycloaddition Chemistry*; Curran, D. P., Ed.; Jai Press: Greenwich, CT, 1993; Vol. 3, pp 99–159.

(6) For recent examples, see: (a) Barr, D. A.; Dorrity, M. J.; Grigg, R.; Malone, J. F.; Montgomery, J.; Rajiviroongit, S.; Stevenson, P. *Tetrahedron Lett.* **1990**, *31*, 6569. (b) Grigg, R.; Markandu, J.; Perrior, T.; Surendrakumar, S.; Warnock, W. J. *Tetrahedron* **1992**, *48*, 6929. (c) Grigg, R.; Montgomery, J.; Somasunderam, A. *Tetrahedron* **1992**, *48*, 10431.

(7) (a) Kanemasa, S.; Yamamoto, H. *Tetrahedron Lett.* **1990**, *31*, 3633. (b) Kanemasa, S.; Tatsukawa, A.; Wada, E. *J. Org. Chem.* **1991**, *56*, 2875.

(8) (a) Annunziata, R.; Cinquini, M.; Cozzi, F.; Raimondi, L.; Pilati, T. *Tetrahedron: Asymmetry* **1991**, *2*, 1329. (b) Patzel, M.; Galley, G.; Jones, P. G.; Chrapkowsky, A. *Tetrahedron Lett.* **1993**, *34*, 5707. (c) Galley, G.; Liebscher, J.; Patzel, M. *J. Org. Chem.* **1995**, *60*, 5005. (d) Rispen, M. T.; Keller, E.; DeLange, B.; Feringa, B. L. *Tetrahedron: Asym* **1994**, *5*, 607. (e) Waldmann, H.; Blaeser, E.; Jansen, M.; Letschert, H. P. *Angew. Chem., Int. Ed. Engl.* **1994**, *33*, 683. (f) Waldmann, H.; Blaeser, E.; Jansen, M.; Letschert, H. P. *Chem. Eur. J.* **1995**, *1*, 150. (g) Pyne, S. G.; Safaei, J.; Koller, F. *Tetrahedron Lett.* **1995**, *36*, 2511.

(9) (a) Gong, Y. D.; Nadji, S.; Olmstead, M. M.; Kurth, M. J. *J. Org. Chem.* **1998**, *63*, 3081. (b) Hamper, B. C.; Dukeshner, D. R.; South, M. S. *Tetrahedron Lett.* **1996**, *37*, 3671. (c) Marx, M. A.; Grillot, A.-L.; Louer, C. T.; Beaver, K. A.; Barlett, P. A. *J. Am. Chem. Soc.* **1997**, *119*, 6153. (d) Murphy, M. M.; Schullek, J. R.; Gordon, E. M.; Gallop, M. A. *J. Am. Chem. Soc.* **1995**, *117*, 7029.

(10) Houk, K. N.; Gonzalez, J.; Li, Y. *Acc. Chem. Res.* **1995**, *28*, 81.

(11) (a) Huisgen, R. In *1,3-Dipolar Cycloaddition Chemistry*; Padwa, A., Ed.; Wiley: New York, 1984; Vol. 1, pp 1–176. (b) Huisgen, R. *J. Org. Chem.* **1976**, *41*, 403. (c) Firestone, R. A.; *J. Org. Chem.* **1968**, *33*, 2285. (d) Firestone, R. A. *Tetrahedron*, **1977**, *33*, 3309.

(12) (a) Huisgen, R. *Angew. Chem., Int. Ed. Engl.* **1963**, *2*, 633. (b) Huisgen, R. *J. Org. Chem.* **1968**, *33*, 2291.

(13) (a) Huisgen, R.; Mloston, G.; Langhals, E. *J. Am. Chem. Soc.* **1986**, *108*, 6401. (b) Mloston, G.; Huisgen, R. *Tetrahedron Lett.* **1989**, *30*, 5373.

(14) Neumann, F.; Lambert, C.; Schleyer, P. v. R. *J. Am. Chem. Soc.* **1998**, *120*, 3357.

no previous theoretical work has been reported for the thermal [3 + 2] cycloaddition between stabilized azomethine ylides and π -deficient alkenes. For the N-metalated version of the reaction only two papers, one from Kanemasa¹⁵ and one from our group¹⁶ have been reported. In these papers, SCF-MO studies using semiempirical Hamiltonians suggest stepwise mechanisms (Scheme 3, path b) for this version of the reaction.

Within this context and in connection with our ongoing program on [3 + 2] cycloadditions,^{16,17} we report herein our study on the reaction between stabilized azomethine ylides and nitroalkenes to yield highly substituted proline derivatives. We have performed computational and experimental studies to exploit the synergy between both approaches. Finally, we have performed a theoretical study to elucidate the reasons underlying the transition from concerted to stepwise mechanisms. The model thus developed can be readily extended to any thermally allowed cycloaddition.

Computational Methods

All of the results presented in this work have been obtained by using the GAUSSIAN 94¹⁸ and GAUSSIAN 98¹⁹ series of programs, with the standard 3-21G(*), 6-31G*, and 6-31+G*²⁰ basis sets. To include electron correlation at a reasonable computational cost, density functional theory (DFT)²¹ has been used. We have used the hybrid three-parameter functional developed by Becke,²² which is usually denoted as B3LYP. Zero-point vibrational energies (ZPVEs), when computed at the HF/3-21G and HF/6-31G* levels were scaled by 0.92 and 0.89, respectively.²³ The ZPVEs computed using the B3LYP functional were not scaled. All transition structures have been fully optimized and characterized by harmonic analysis. For each located transition structure, only one imaginary frequency was found in the diagonalized Hessian matrix, and the corresponding vibration was found to be associated with nuclear motion along the reaction coordinate under study. In

(15) Tatsukawa, A.; Kawatake, K.; Kanemasa, S.; Rudzinski, J. M. *J. Chem. Soc., Perkin Trans. 2* **1994**, 2525.

(16) Ayerbe, M.; Arrieta, A.; Cossío, F. P.; Linden, A. *J. Org. Chem.* **1998**, *63*, 1795.

(17) (a) Morao, I.; Lecea, B.; Cossío, F. P. *J. Org. Chem.* **1997**, *62*, 7033. (b) Morao, I.; Cossío, F. P. *J. Org. Chem.* **1999**, *64*, 1868. (c) Cossío, F. P.; Morao, I.; Jiao, H.; Schleyer, P. v. R. *J. Am. Chem. Soc.* **1999**, *121*, 6737.

(18) Frisch, M. J.; Trucks, G. W.; Schlegel, H. B.; Gill, P. M. W.; Johnson, B. G.; Robb, M. A.; Cheeseman, J. R.; Keith, T.; Petersson, G. A.; Montgomery, J. A.; Raghavachari, K.; Al-Laham, M. A.; Zakrzewski, V. G.; Ortiz, J. V.; Foresman, J. B.; Peng, C. Y.; Ayala, P. Y.; Chen, W.; Wong, M. W.; Andres, J. L.; Replogle, E. S.; Gomperts, R.; Martin, R. L.; Fox, D. J.; Binkley, J. S.; Defrees, D. J.; Baker, J.; Stewart, J. S.; Head-Gordon, M.; Gonzalez, C.; Pople, J. A. *Gaussian 94*, revision B.2.; Gaussian, Inc.: Pittsburgh, PA, 1995.

(19) Frisch, M. J.; Trucks, G. W.; Schlegel, H. B.; Scuseria, G. E.; Robb, M. A.; Cheeseman, J. R.; Zakrzewski, V. G.; Montgomery, J. A., Jr.; Stratmann, R. E.; Burant, J. C.; Dapprich, S.; Millam, J. M.; Daniels, A. D.; Kudin, K. N.; Strain, M. C.; Farkas, O.; Tomasi, J.; Barone, V.; Cossi, M.; Cammi, R.; Mennucci, B.; Pomelli, C.; Adamo, C.; Clifford, S.; Ochterski, J.; Petersson, G. A.; Ayala, P. Y.; Cui, Q.; Morokuma, K.; Malick, D. K.; Rabuck, A. D.; Raghavachari, K.; Foresman, J. B.; Cioslowski, J.; Ortiz, J. V.; Stefanov, B. B.; Liu, G.; Liashenko, A.; Piskorz, P.; Komaromi, I.; Gomperts, R.; Martin, R. L.; Fox, D. J.; Keith, T.; Al-Laham, M. A.; Peng, C. Y.; Nanayakkara, A.; Gonzalez, C.; Challacombe, M.; Gill, P. M. W.; Johnson, B.; Chen, W.; Wong, M. W.; Andres, J. L.; Gonzalez, C.; Head-Gordon, M.; Replogle, E. S.; Pople, J. A. *Gaussian 98*, revision A.5; Gaussian, Inc.: Pittsburgh, PA, 1998.

(20) Hehre, W. J.; Radom, L.; Schleyer, P. v. R.; Pople, J. A. *Ab Initio Molecular Orbital Theory*; Wiley: New York, 1986; pp 76–87 and references therein.

(21) Parr, R. G.; Yang, W. *Density-Functional Theory of Atoms and Molecules*; Oxford: New York, 1989.

(22) (a) Kohn, W.; Becke, A. D.; Parr, R. G. *J. Phys. Chem.* **1996**, *100*, 12974. (b) Becke, A. D. *J. Chem. Phys.* **1993**, *98*, 5648. (c) Becke, A. D. *Phys. Rev. A* **1988**, *38*, 3098.

(23) Pople, J. A.; Schlegel, H. B.; Krishnan, R.; De Fries, D. J.; Binkley, J. S.; Frisch, H.; Whiteside, R.; Hout, R. F., Jr.; Hehre, W. J. *Int. J. Quantum Chem. Symp.* **1981**, *15*, 269.

several significant cases intrinsic reaction coordinate (IRC)²⁴ calculations were performed to connect unambiguously transition structures with reactants, cycloadducts and reaction intermediates.

Bond orders and atomic charges were calculated with the natural bond orbital (NBO) method.²⁵

Nonspecific solute–solvent interactions were simulated using either the Onsager–Kirkwood^{26,27} or the self-consistent isodensity polarization models (SCIPCM)²⁸ as implemented by Wiberg.²⁹

In several cases (vide infra) molecular mechanics computations were performed on several stationary points in order to determine the minimum energy conformations. These calculations were performed using the AMBER³⁰ force field as implemented in the MacroModel³¹ package. The different possible conformers were optimized and then Monte Carlo³² simulations were performed on 1000 structures.

Atoms-in-molecules (AIM)³³ calculations were performed with the AIMPAC³⁴ program. Nucleus-independent chemical shifts (NICS),³⁵ were calculated by means of the gauge-independent atomic orbitals³⁶ (GIAO) method. The synchronicity parameter denoted in the text as S_y has been computed using the proposal of Pericàs and Moyano³⁷ and according to the methodology previously reported by our group.³⁸ For a perfectly synchronous reaction, $S_y = 1$ and for a completely asynchronous reaction $S_y = 0$.

Results and Discussion

Lithium Azomethines. We have studied first the structure and the properties of lithium azomethine **1a** both in the gas phase and in acetonitrile solution ($\epsilon = 35.94$).³⁹ All of the possible conformations have been analyzed, and their relative energies are reported in Table 1. From our calculated energies it is concluded that these stabilized lithium azomethines exist exclusively in the conformation **A**, in which lithium interacts with both the nitrogen and oxygen atoms. Figure 1A shows the main geometric data of **1a** in this conformation. An analysis of the energy densities $H(\mathbf{r}_c)$ at the corresponding critical points⁴⁰ reveals that the lithium–heteroatom interactions are electrostatic

(24) Gonzalez, C.; Schlegel, H. B. *J. Phys. Chem.* **1990**, *94*, 5523.

(25) (a) Reed, A. E.; Curtiss, L. A.; Weinhold, F. *Chem. Rev.* **1988**, *88*, 899. (b) Reed, A. E.; Weinstock, R. B.; Weinhold, F. *J. Chem. Phys.* **1985**, *83*, 735.

(26) (a) Onsager, L. *J. Am. Chem. Soc.* **1936**, *58*, 1486. (b) Wong, M. W.; Wiberg, K. B.; Frisch, M. J. *J. Am. Chem. Soc.* **1992**, *114*, 523.

(27) As one reviewer has indicated, this is an approximation of the solvation energy. Similarly, the ϵ function is a very crude estimate of solvent polarity. See ref 46 for more detailed treatment of this problem. See also: Huisgen, R. *Pure Appl. Chem.* **1981**, *53*, 171 and references therein.

(28) Tomasi, J.; Persico, M. *Chem. Rev.* **1994**, *94*, 2027.

(29) (a) Wiberg, K. B.; Castejon, H.; Keith, T. A. *J. Comput. Chem.* **1996**, *17*, 185. (b) Wiberg, K. B.; Rablen, P. R.; Rush, D. J.; Keith, T. A. *J. Am. Chem. Soc.* **1995**, *117*, 4261.

(30) Cornell, W. D.; Cieplak, P.; Bayly, C. I.; Gould, I. R.; Merz, K. M., Jr.; Ferguson, D. M.; Spellmeyer, D. C.; Fox, T.; Caldwell, J. W.; Kollman, P. A. *J. Am. Chem. Soc.* **1995**, *117*, 5179.

(31) *MacroModel*, v5.0. Mohamadi, F.; Richards, N. G. J.; Guida, W. C.; Liskamp, R.; Lipton, M.; Caufield, C.; Chang, G.; Hendrickson, T.; Still, W. C. *J. Comput. Chem.* **1990**, *11*, 440.

(32) (a) Chang, G.; Guida, W. C.; Still, W. C. *J. Am. Chem. Soc.* **1989**, *111*, 4379. (b) Saunders: M., Houk, K. N.; Wu, Y.-D.; Still, W. C.; Lipton, M.; Chang, G.; Guida, W. *J. Am. Chem. Soc.* **1990**, *119*, 1419.

(33) Bader, R. F. W. *Atoms in Molecules. A Quantum Theory*; Clarendon Press: Oxford, 1990.

(34) Cheeseman, J.; Keith, T.; Bader, R. F. W. *AIMPAC v2.0*; McMaster University: Hamilton, Ontario L8S 4M1, Canada.

(35) Schleyer, P. v. R.; Maerker, C.; Dransfeld, A.; Jiao, H.; Hommes, N. J. R. V. E. *J. Am. Chem. Soc.* **1996**, *118*, 6317.

(36) Wolinski, K.; Hilton, J. F.; Pulay, P. *J. Am. Chem. Soc.* **1990**, *112*, 8251.

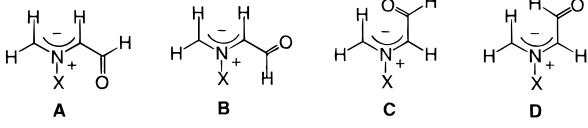
(37) Moyano, A.; Pericàs, M. A.; Valentí, E. *J. Org. Chem.* **1989**, *54*, 573.

(38) (a) Lecea, B.; Arrieta, A.; Roa, G.; Ugalde, J. M.; Cossío, F. P. *J. Am. Chem. Soc.* **1994**, *116*, 9613. (b) Lecea, B.; Arrieta, A.; Lopez, X.; Ugalde, J. M.; Cossío, F. P. *J. Am. Chem. Soc.* **1995**, *117*, 12314.

(39) Reichardt, C. *Solvents and Solvent Effects in Organic Chemistry* VCH: Weinheim, 1990; pp 408–410.

(40) Cremer, D.; Kraka, E. *Croat. Chem. Acta* **1989**, *57*, 1259.

Table 1. Relative Energies^{a,b} (kcal/mol) of the Conformations of Azomethine Ylides **1a,c**



conformation	$\epsilon = 1.00$		$\epsilon = 35.94$	
	1a (X = Li)	1c (X = H)	1a (X = Li)	1c (X = H)
A	0.0	0.0	0.0	0.0
B	31.4	5.5	<i>c</i>	3.6
C	34.0	2.8	19.5	2.8
D	38.4	9.3	14.9	6.7

^a Relative energies with respect to conformation **A**. ^b Values computed at the MP2/6-31+G*/HF/6-31+G*+ Δ ZPVE and the MP2(L1A1)/6-31+G*/HF(L1A1)/6-31+G*+ Δ ZPVE levels. ^c The starting geometries converged to conformation **A** upon optimization.

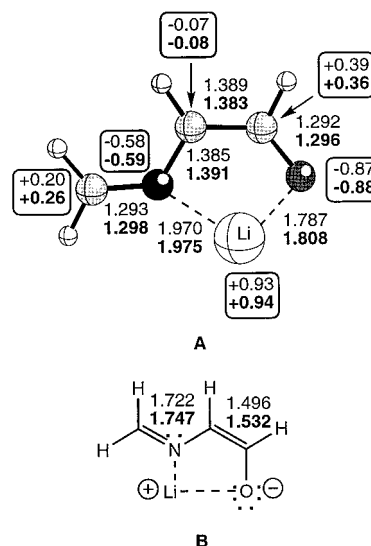
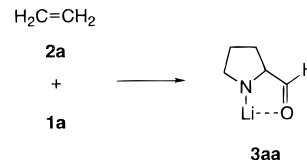


Figure 1. B3LYP/6-31+G* (plain text) and B3LYP(L1A1)/6-31+G* ($\epsilon = 35.94$, bold text) fully optimized geometry of the most stable conformation of lithium azomethine **1a**. (A) Bond distances (Å) and NBO charges (au, boxed numbers). (B) Wiberg bond indices. In this and the following figures which incorporate ball-and-stick drawings, atoms are represented by increasing order of shadowing as follows: H, C, O, N.

Scheme 4



in nature.⁴¹ This result, together with the NBO analysis, leads to the valence-bond structure depicted in Figure 1B. According to these results, the structure of **1a** is closer to that of an enolate than to that of an azomethine ylide.

We have also studied the interaction between lithium azomethine **1a** and ethylene **2a** to yield the lithium amide **3aa** (Scheme 4). This model reaction represents the simplest [3 + 2] cycloaddition between a lithium stabilized azomethine ylide and an alkene. The main geometric features of the stationary points found in the B3LYP/6-31+G* potential energy hypersurfaces,

(41) (a) Lecea, B.; Arrieta, A.; Morao, I.; Cossío, F. P. *Chem. Eur. J.* **1997**, *3*, 20. (b) Lopez, X.; Ugalde, J. M.; Cossío, F. P. *J. Am. Chem. Soc.* **1996**, *118*, 2718.

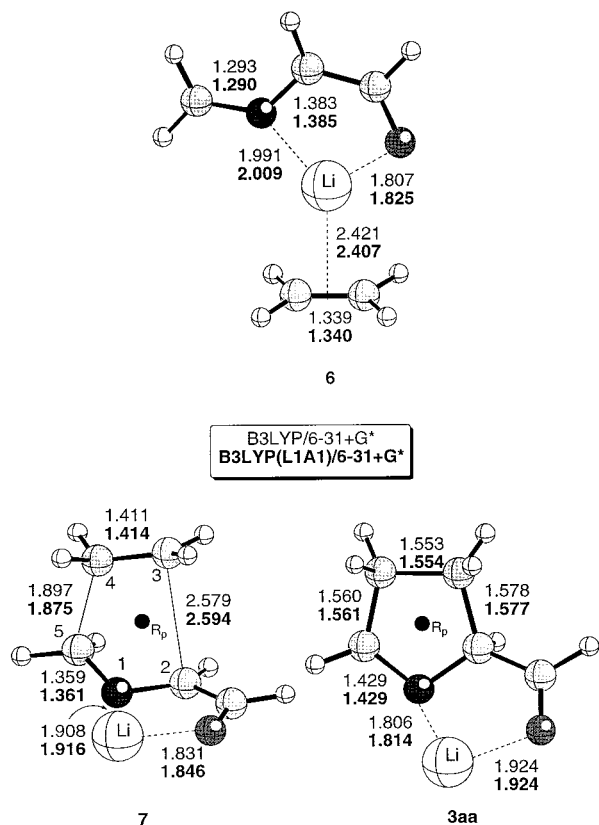


Figure 2. Main geometric features of the stationary points found in the $1a + 2a \rightarrow 3aa$ reaction (see Scheme 4), computed in the gas phase and in acetonitrile solution. Bond distances are given in Å. R_p denotes the (3,+1) ring point of the electron density. See the caption of Figure 1.

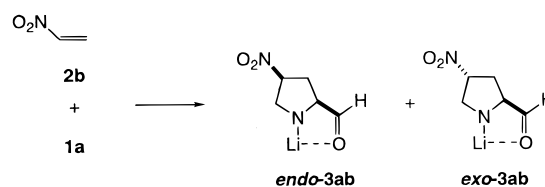
Table 2. Complexation Energies^a (ΔE_c , kcal/mol), Activation Energies^b (ΔE_a , kcal/mol), and Reaction Energies^c (ΔE_{rxn} , kcal/mol) of the $1a + 2a \rightarrow 3aa$ Reaction^d (see Scheme 4)

method	ΔE_c	ΔE_a	ΔE_{rxn}
HF/6-31+G*	-6.6	52.4	-3.9
MP2/6-31+G* ^e	-9.7	24.8	-12.9
B3LYP/6-31+G*	-7.3	31.5	-0.4
B3LYP(L1A1)/6-31+G* ^f	-6.8	32.7	-2.6

^a Computed as $\Delta E_c = E(6) - [E(1a) + E(2a)]$. ^b Computed as $\Delta E_a = E(7) - E(6)$. ^c Computed as $\Delta E_{rxn} = E(3a) - [E(1a) + E(2a)]$. ^d The zero-point energy corrections, conveniently scaled if necessary (see text) were computed at the geometry optimization level. ^e Single-point energy computed on the HF/6-31+G* optimized structures. ^f The energy differences in solution were computed in acetonitrile ($\epsilon = 35.94$).

both in the gas phase and in simulated acetonitrile solution are depicted in Figure 2. The corresponding relative energies are reported in Table 2. The first step of this reaction is found to consist of the formation of an orientation complex resulting from the coordination of the lithium cation of $1a$ with the ethylene unit. From **6**, the next stationary point is **7**, that corresponds to a concerted *supra-supra* interaction between $1a$ and $2a$. The AIM analysis of the electron density shows a (3,+1) ring point (R_p) in **7**. In addition, the NICS computed at the ring point is found to be $-20.44 \text{ ppm mol}^{-1}$ at the SCF-GIAO/6-31+G**/B3LYP/6-31+G* level. This result indicates that this transition structure is in-plane aromatic.¹⁷ However, the computed synchronicity (S_y) for the $1a + 2a \rightarrow 3aa$ transformation is calculated to be $S_y = 0.66$ at the B3LYP/6-31+G* level. As can be seen in Figure 2, the large difference between the C4...C5 and C3...C2 bonds is responsible for this quite low synchronicity. In summary, the reaction between $1a$ and ethylene

Scheme 5^a



^a Only one enantiomer is drawn.

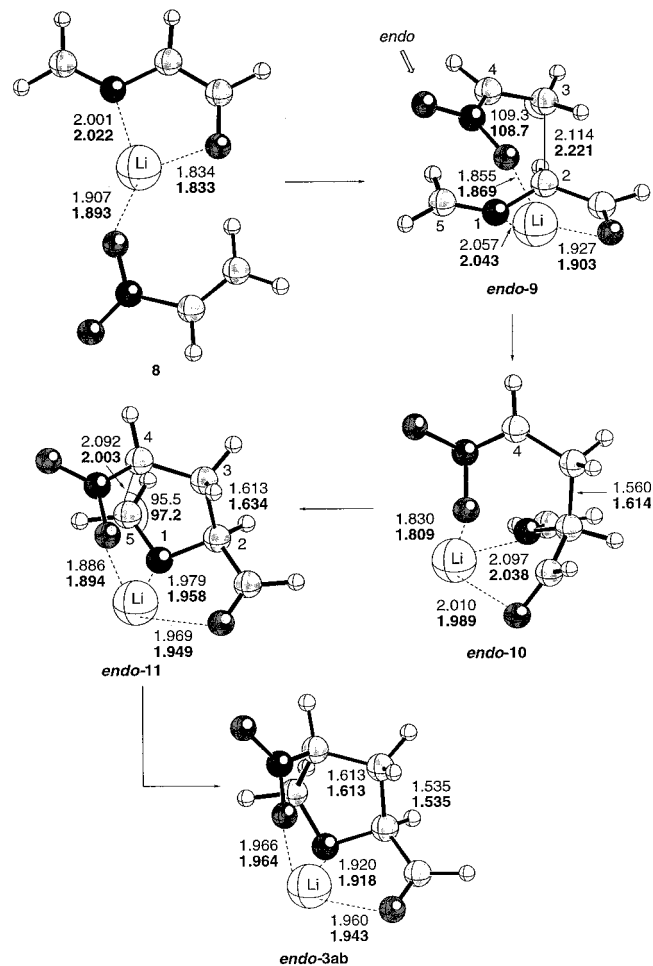


Figure 3. Main geometric features of the stationary points found in the $1a + 2b \rightarrow \text{endo-3ab}$ transformation (see Scheme 5). See the captions of Figures 1 and 2.

is predicted to be a concerted, although quite asynchronous, [3 + 2] cycloaddition, despite the considerable enolate-like character of $1a$. This results in a quite large activation energy, as can be appreciated from Table 2. Therefore, it is expected that the substituent effect in this reaction could induce considerable changes in the reaction profile.

Since the nitro group is one of the most versatile^{16,42} electron-withdrawing groups (EWG), we next computed the interaction between $1a$ and nitroethylene $2b$ (Scheme 5) to yield the cycloadducts **3ab**. In this case, formation of two diastereomers is possible. We shall denote the *endo* structures as those in which both EWGs are in a cis relationship. If these groups are trans to each other, the corresponding structure shall be denoted *exo* (Scheme 5).

(42) (a) Efremov, D. A.; Berestovitskaya, V. M.; Perekalin, V. V. *Nitroalkenes; Conjugated Nitro Compounds*; Wiley: Chichester, 1994. (b) Barrett, A. G. M.; Grabosky, G. G. *Chem. Rev.* **1986**, *86*, 751. For [3 + 2] cycloadditions between azomethine ylides and nitro-olefins see: Pak, C. S.; Nyerges, M. *Synlett* **1999**, 1271 and references therein.

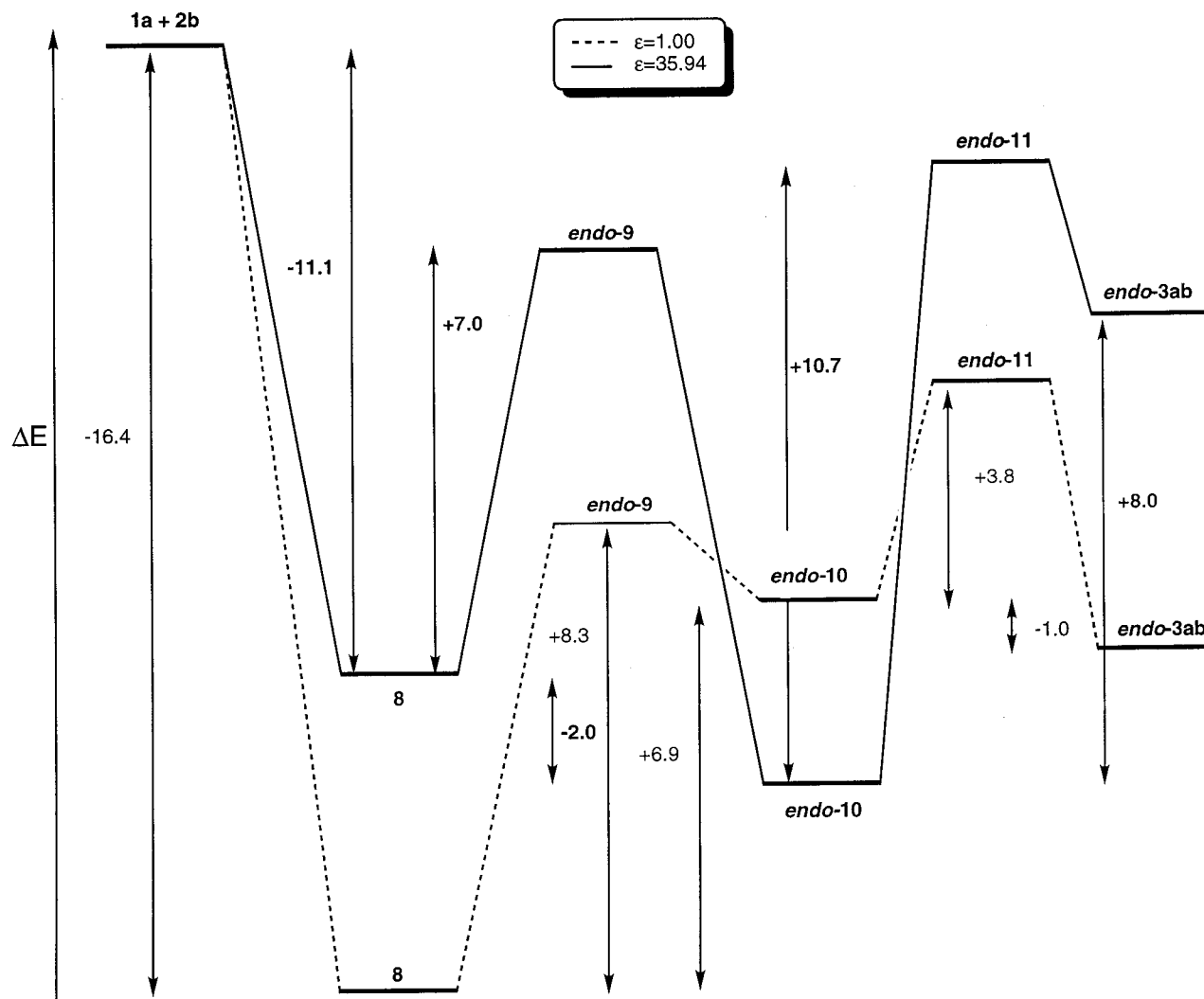


Figure 4. Reaction profiles found in vacuo and in acetonitrile solution ($\epsilon = 35.94$) for the $1a + 2b \rightarrow \text{endo-3ab}$ transformation. Zero point vibrational energies have been included. The plain numbers correspond to the gas-phase results.

All of our attempts to locate concerted transition structures, as we did in the $1a + 2a \rightarrow 3aa$ cycloaddition, were unfruitful. Instead, we found stepwise mechanisms in the B3LYP/6-31+G* potential energy surface, both in the gas phase and in acetonitrile solution. The stationary points which were located and characterized are shown in Figure 3, and the corresponding reaction profile is depicted in Figure 4.

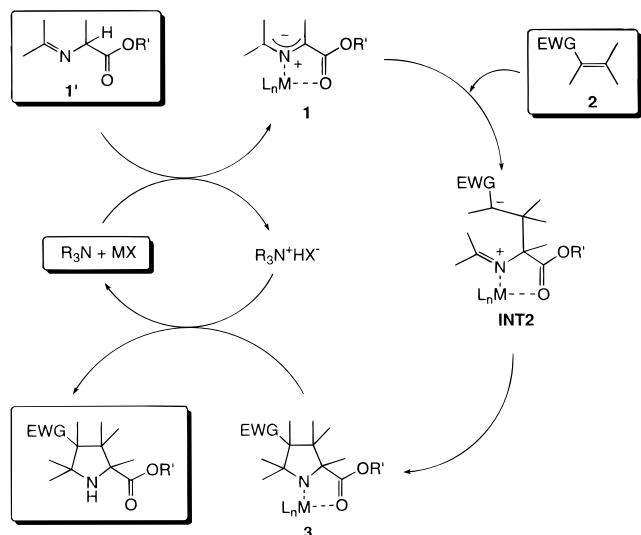
The first reaction intermediate is the result of the interaction between the lithium cation of **1a** and one of the two oxygen atoms of the nitro group of **2b**. **8** is ~ 5 kcal/mol less stable in solution than in the gas phase (See Figure 4), but the complexation energy is still appreciable.

We have also located a first transition structure *endo-9* leading to the formation of the C2–C3 bond. This distance is slightly shorter than that found in **7**. However, there is no appreciable interaction between C4 and C5 and the C2...C3–C4 angle of attack is found to be $\sim 109^\circ$ (See Figure 3). Therefore, this transition structure does not correspond to a concerted *supra-supra* mechanism but to a nucleophilic Michael-type addition in which **1a** behaves as a lithium enolate. In addition, in *endo-9* there is an electrostatic interaction between one of the oxygen atoms of the nitro group and the lithium atom. This additional stabilizing interaction is kept along the reaction coordinate thus leading to *endo-3ab*. The alternative *exo* stationary points are considerably higher in energy (~ 10 – 20 kcal/mol along the reaction coordinate in the gas phase) since in those diastereo-

meric structures the Coulombic Li...ONO interaction is not present (see Figures S1 and S2 of the Supporting Information). Therefore, a high stereocontrol can be expected for this reaction despite the stepwise nature of its mechanism. This is a remarkable prediction since stereochemical arguments have been crucial in the elucidation of concerted or stepwise mechanisms in other [3 + 2] cycloadditions.⁴³ Another interesting point is that, according to our calculations, solvent effects accelerate this reaction step. Thus, in the $1a + 2b \rightarrow \text{endo-3ab}$ transformation the activation barrier associated with the formation of the C2–C3 bond is calculated to be ~ 1.33 kcal/mol lower than in vacuo (See Figure 4).

The next point along the reaction coordinate is *endo-10*, in which the C2–C3 bond is formed. In this local minimum there is a considerable double bond character between C4 and the nitro group, with a NBO bond order value of 1.44 (B3LYP-(L1A1)/6-31+G* level). The calculated charge for the nitro group is -0.96 e. Therefore, *endo-10* corresponds to a zwitterionic intermediate in which the anionic part is a nitronate moiety and the positive part corresponds to an iminium cation. Since the charge separation is difficult in the gas phase, this

(43) (a) Bihlmaier, W.; Geittner, J.; Huisgen, R.; Reissig, H.-V. *Heterocycles* **1978**, *10*, 147. (b) Van Auken, T. V.; Rinehart, K. L. *J. Am. Chem. Soc.* **1962**, *84*, 3736. (c) Houk, K. N.; Firestone, R. A.; Munchausen, L. L.; Mueller, P. H.; Arison, B. H.; Garcia, L. A. *J. Am. Chem. Soc.* **1985**, *107*, 7227.

Scheme 6^a

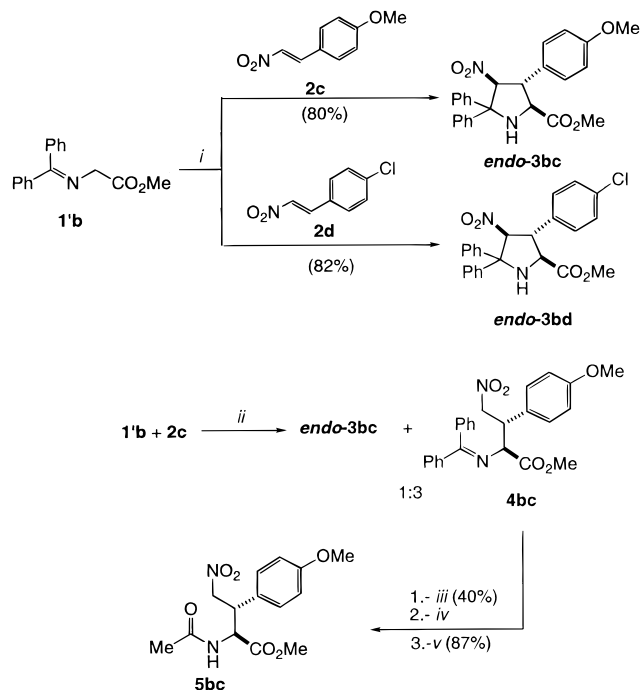
^a The usually isolated species correspond to the boxed structures. L_n represents solvent molecules or other ligands coordinated to the metal.

zwitterionic intermediate is highly stabilized in solution with respect to the gas phase (Figure 4), although the geometric features are quite similar in both media (Figure 3).

The second transition structure *endo-11* leads to the formation of the C4–C5 bond and its geometric features correspond to nitroaldol-like process,^{41a} with a half-chair conformation for the Li–N1–C2–C5–O moiety (See Figure 3). Again, although the in vacuo and acetonitrile solution geometries of this saddle point are quite similar, the activation barrier is ~ 7 kcal/mol larger in solution than in the gas phase, because of the large stabilization of *endo-10* in solution. This result is due to the partial cancellation in the *endo-11* structure of the charge separation present in the zwitterionic intermediate.

Finally, we have characterized the N-lithiated cycloadduct *endo-3ab*, which lies 2.7 kcal/mol below *endo-11* in acetonitrile solution (Figure 4). This reaction product is ~ 8 kcal/mol less stable than *endo-10* in solution, a result which explains why, in several cases, reaction products derived from intermediates of this kind have been reported.^{16,44} In this respect, it is noteworthy that in many experimental studies the N-metalated azomethines are generated using catalytic amounts of salts in the presence of bases such as tertiary amines.^{2b,c,8} Our results indicate that the reaction mechanism coupled with the catalytic cycle is that depicted in Scheme 6. Thus, the N-metalated azomethine ylide is generated in situ from an imine and then interacts with the alkene to yield the N-metalated cycloadduct via the corresponding zwitterionic intermediate. Then, the catalytic system is regenerated via proton transfer from the ammonium ion to the pyrrolidine ring.

Since our calculations indicate that in the stepwise reaction between **1a** and **2b** the key intermediate *endo-10* lies in a deep enough well, we thought that its evolution should be detectable by NMR monitoring, provided that the substituents present in the starting materials were appropriate. Therefore, we decided

Scheme 7^a

^a Reagents and conditions: i: LiClO₄ (1 equiv), NEt₃ (1.0 equiv), CH₃CN, 24 h, rt. ii: LiClO₄ (1.0 equiv), NEt₃ (1.0 equiv), CH₃CN, 60 min, rt. iii: THF, HCl 2 N, 20 min, rt. iv: CF₃CO₂H, CH₂Cl₂, 5 h, rt. v: Ac₂O (1.5 equiv), NEt₃ (1.6 equiv), CH₂Cl₂, 48 h, rt. ^b In the chiral structures only one enantiomer is drawn.

to study the reaction between imine **1'b** and nitroalkenes **2c,d** which yields pyrrolidines **3bc** and **3bd**, respectively (Scheme 7). We chose this particular imine because, according to our computational studies, if the zwitterionic intermediates were formed, the two phenyl groups should stabilize the positive charge of the iminium fragment. Therefore, the second step, namely the nitroaldol-like process should be slower. We first performed the two cycloadditions, reported in Scheme 7, using lithium perchlorate as the lithium source and triethylamine as the base. The solvent was acetonitrile, the same one used in the calculations. After 24 h of reaction, the *endo* cycloadducts **3bc** and **3bd** were obtained in good yields. The *endo* stereochemistry was assigned on the basis of the values of the ³J_{2,3} coupling constants (4.0 Hz).¹⁶ In addition, the structure of *endo-3bc* was confirmed by X-ray diffraction analysis⁴⁵ (see Supporting Information). Therefore, the *endo* isomer was observed in these cases, as predicted by the calculations.

We also monitored the reaction mixture of the **1'b** + **2c** → *endo-3bc* transformation at different times in order to observe the presence of the corresponding Michael intermediate. The results of this study are displayed in Figure 5A. As diagnostic signals we monitored the resonances of the methinic protons contiguous to the nitro group as shown in Figure 5B. The structure of intermediate **4bc** was confirmed by isolation and derivatization to the stable and crystalline N-acyl derivative **5bc** (See Scheme 7), whose structure was also determined by X-ray

(44) (a) Tsuge, O.; Kanemasa, S.; Ohe, M.; Yorozu, K.; Takenaka, S.; Ueno, K. *Chem. Lett.* **1986**, 1271. (b) Kanemasa, S.; Yoshioka, M.; Tsuge, O. *Bull. Chem. Soc. Jpn* **1989**, 62, 869. (c) Werf, A.; Kellogg, R. M. *Tetrahedron Lett.* **1991**, 32, 3727. (d) Kanemasa, S.; Kumegawa, E.; Wada, E.; Nomura, M. *Bull. Chem. Soc. Jpn* **1991**, 64, 2990. (e) Chavan, S. P.; Venkatraman, M. S.; Shama, A. K.; Chittiboyina, A. G. *Tetrahedron Lett.* **1996**, 37, 2857. (f) Rowley, M.; Leeson, P. D.; Williams, B. J.; Moore, K. W.; Baker, R. *Tetrahedron* **1992**, 48, 3557.

(45) Crystal data for *endo-3bc*: C₂₅H₂₄N₂O₅, $M_r = 432.47$, orthorhombic, P2₁2₁2₁, colorless prism (0.35 × 0.45 × 0.45 mm), $a = 10.797(2)$ Å, $b = 22.824(4)$ Å, $c = 8.768(3)$ Å, $V = 2160.7(8)$ Å³, $Z = 4$, $d_{\text{calc}} = 1.329$ g cm⁻³, $\mu = 0.0932$ mm⁻¹, $T = 173(1)$ K, Mo K α radiation ($\lambda = 0.71069$ Å), Rigaku AFC5R diffractometer, ω/θ scans. Refinement on F gave $R = 0.0399$, $wR = 0.0359$, GOF = 1.767 using 294 refined parameters and 2594 observed reflections with $I > 2\sigma(I)$ from the 3333 collected (3219 unique) with $2\theta < 55^\circ$. The structure was solved by direct methods and all non-hydrogen atoms were refined anisotropically.

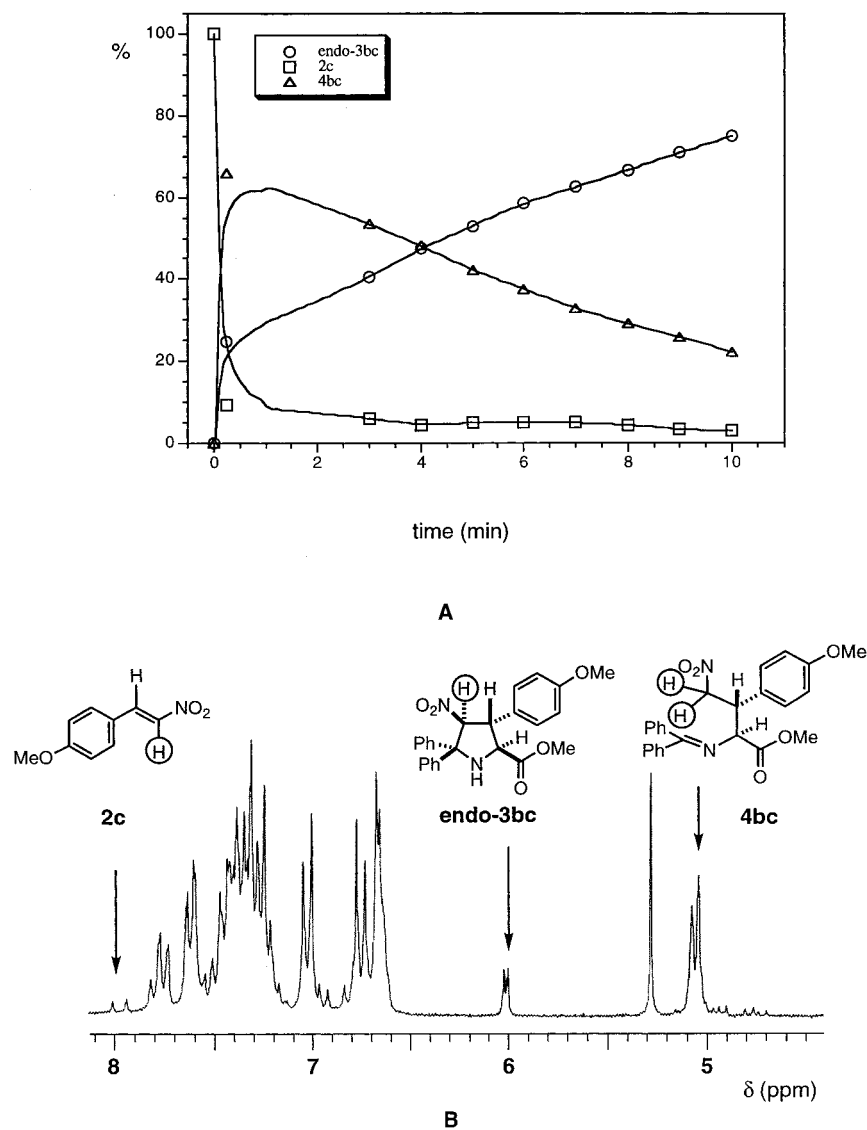


Figure 5. (A) Plot of the reaction mixture in the $1'b + 2c \rightarrow \text{endo-3bc}$ reaction against the reaction time. (B) An example of the 300 MHz ^1H NMR spectra of the reaction mixture showing the diagnostic signals of the different species.

analysis (see Supporting Information).⁴⁶ Therefore, the curves of Figure 5A confirm that this reaction is stepwise as suggested by the previous computational study. To test if the first step of the reaction is irreversible, after 60 min of reaction, we added nitroalkene **2d**, more electrophilic than **2c**, to a reaction mixture of **1'b** and **2c**. After 24 h of reaction at room temperature, only cycloadduct **endo-3bc** was obtained, with no detectable amounts of **endo-3bd**.

N-Protonated Azomethine Ylides. Since such compounds are usually generated in situ from the corresponding imines,^{2b,c,5} we have studied this previously reported transformation first. The main geometric features of imine **1'c** and its azomethine ylide **1c** are displayed in Figure 6.

The transition structure **12** which connects both isomers via a 1,2-proton shift is also reported in the same Figure. The

corresponding activation energy is calculated to be 57.8 kcal/mol in the gas phase (See Table 3), a quite large value. Inclusion of one *p* polarization function in the migrating hydrogen atom lowers the activation energy 2.7 kcal/mol. Another possibility for this transformation consists of the enolization of the imine to the corresponding enol imine **1''c** (Figure 6). In general, enolization is a complex process in which general acid and base catalysis⁴⁷ as well as solvent⁴⁸ and tunneling⁴⁹ effects are important. We have computed the relative energies between **1'c** and **1''c** in the gas phase and in several solvents. The results are included in Table 3. Although direct comparison with experimental values is not possible, the magnitude of the energy differences is in line with experimental values obtained on related compounds. For instance, it has been reported⁵⁰ that 3-hydroxypyrrole is ~ 1.2 kcal/mol less stable than 3-ketopyrrole in water at 298 K.

(46) Crystal data for **5bc**: $\text{C}_{14}\text{H}_{18}\text{N}_2\text{O}_6$, $M_r = 310.30$, monoclinic, $P2_1/c$, colorless plate ($0.14 \times 0.32 \times 0.45$ mm), $a = 10.600(1)$ Å, $b = 15.514(2)$ Å, $c = 10.014(2)$ Å, $V = 1531.3(4)$ Å³, $Z = 4$, $d_{\text{calc}} = 1.346$ g cm⁻³, $\mu = 0.106$ mm⁻¹, $T = 173(1)$ K, Mo $K\alpha$ radiation ($\lambda = 0.71069$ Å), Rigaku AFC5R diffractometer, $\omega/2\theta$ scans. Refinement on F gave $R = 0.0589$, $wR = 0.0463$, GOF = 1.686 using 203 refined parameters and 1806 observed reflections with $I > 2\sigma(I)$ from the 3838 collected (3506 unique) with $2\theta < 55^\circ$. The structure was solved by direct methods and all non-hydrogen atoms were refined anisotropically.

(47) (a) Hart, H. *Chem. Rev.* **1979**, *79*, 515. (b) Bruice, P. Y.; Bruice, T. C. *J. Am. Chem. Soc.* **1976**, *103*, 1761.

(48) Capon, B.; Rycroft, D. S.; Watson, T. W.; Zucco, C. *J. Am. Chem. Soc.* **1981**, *103*, 1761.

(49) Bell, R. L.; Taveras, D. L.; Truong, T. N.; Simons, J. *J. Comput. Chem.* **1997**, *63*, 861.

(50) Capon, B.; Guo, B.-Z.; Kwok, F. C.; Siddhanta, A. K.; Zucco, C. *Acc. Chem. Res.* **1988**, *21*, 135.

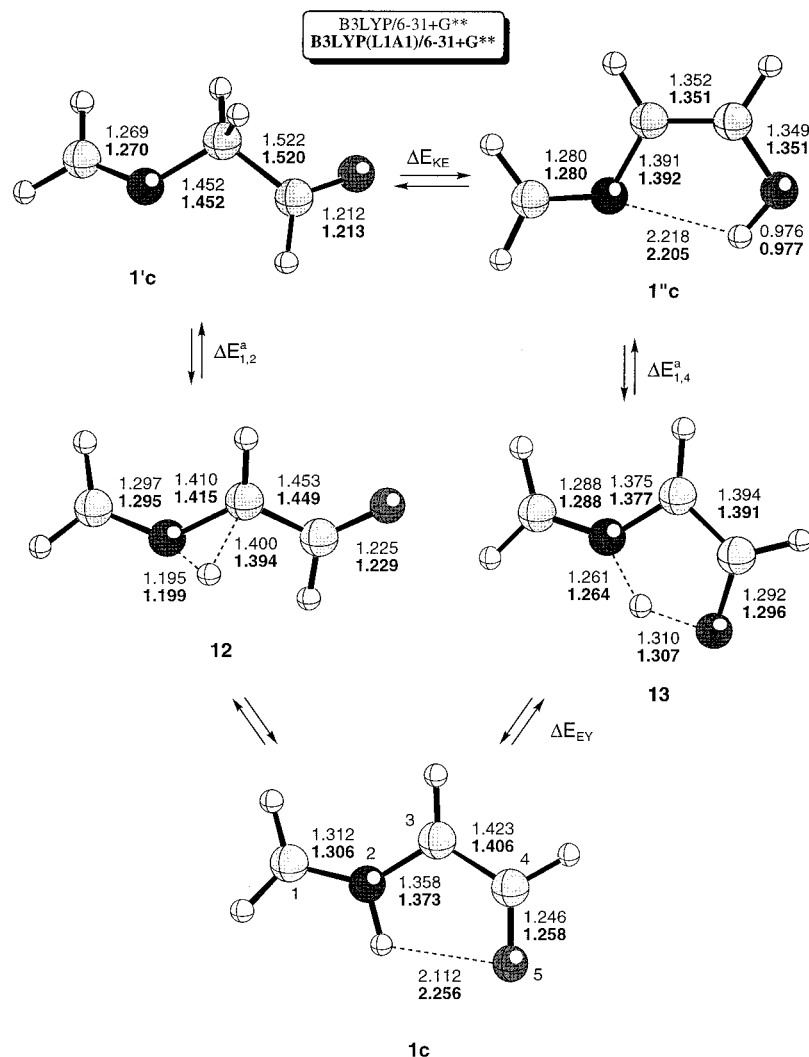


Figure 6. Main geometric features of the stationary points found in the formation of 1,3-dipole **1c** from imine **1'c**. See the captions of Figures 1 and 2.

Table 3. Keto–Enol Energies^{a,b} (ΔE_{KE} , kcal/mol), Enol–Azomethine Energies^{a,c} (ΔE_{EY} , kcal/mol), and Activation Energies^{a,d} ($\Delta E_{1,2}^a$ and $\Delta E_{1,4}^a$, kcal/mol) Associated with the Formation of Azomethine **1c** in Different Solvents

solvent	ϵ	ΔE_{KE}	ΔE_{EY}	$\Delta E_{1,2}^a$	$\Delta E_{1,4}^a$
gas phase	1.00	-0.3 (2.4) ^e	5.5 (7.3) ^e	55.2 (57.8) ^e	12.3 (13.2) ^e
C ₆ H ₅ CH ₃	2.38	-0.1 (2.7) ^e	6.8 (8.4) ^e	54.2 (56.8) ^e	12.1 (12.6) ^e
C ₆ H ₅ Br	5.40	0.1	8.0	53.4	11.8
<i>o</i> -C ₆ H ₄ Cl ₂	9.93	0.3	8.8	53.0	11.6
C ₆ H ₅ CN	34.78	0.4	9.1	52.6	11.5

^a Computed at the B3LYP/6-31+G** + $\Delta ZPVE$ and the B3LYP-(L1A1)/6-31+G** + $\Delta ZPVE$ levels in vacuo and in solution, respectively. ^b Computed as $\Delta E_{KE} = E(\mathbf{1}'c) - E(\mathbf{1}c)$. ^c Computed as $\Delta E_{EY} = E(\mathbf{13}) - E(\mathbf{1}c)$. ^d Computed as $\Delta E_{1,4}^a = E(\mathbf{13}) - E(\mathbf{1}'c)$ and $\Delta E_{1,2}^a = E(\mathbf{12}) - E(\mathbf{1}'c)$, respectively. ^e Values calculated at the B3LYP/6-31+G* + $\Delta ZPVE$ and the B3LYP(L1A1)/6-31+G* + $\Delta ZPVE$ levels in vacuo and in solution, respectively.

We have located and characterized the transition structure **13** which connects **1'c** with **1c**. As can be seen from Figure 6, both **1c** and **1'c** correspond to the two minima of the intramolecular O···H···N bond, with the enol being favored (see Table 3). Therefore, our calculations suggest that the generation of *N*-unsubstituted azomethine ylides takes place via keto–enol tautomerization of the starting imines followed by isomerization

via transition structures related to **13**. Given the lack of experimental data, it is difficult to assess which step is kinetically more relevant, although on the basis of experimental studies on related systems,^{47,48,50} it can be suggested that generation of **1c** is the limiting step.

The conformational equilibrium of azomethine ylide **1c** is similar to that previously found for **1a**, although the energy differences are smaller. Again, the conformation **A** is the most stable one, both in the gas phase and in solution (see Table 1), mainly because of the intramolecular hydrogen bond present in this conformer. The chief geometric features of **1c** are also reported in Figure 6. Interestingly, the coefficients of the HOMO of **1c** are those that might be expected for a 1,3-dipole, with a ratio between C1 and C3 of

$$\frac{c_3}{c_1} = \frac{f_3^-}{f_1^-} = \frac{S_3^-}{S_1^-} = 1.13$$

where c_1 and c_3 are the expansion coefficients of the 1 and 3 carbon atoms (Figure 6). Similarly, f_1^- and S_1^- are the nucleophilic Fukui functions and local softnesses of the same atoms, respectively. In the case of **1a**, this ratio was found to be 1.35. This result and the NBO charges indicate that **1c** is closer to a standard 1,3-dipole than **1a**.

Next, we studied the interaction between dipole **1c** and ethylene **2a** to yield pyrrolidine **3ca** (Scheme 8). The stationary

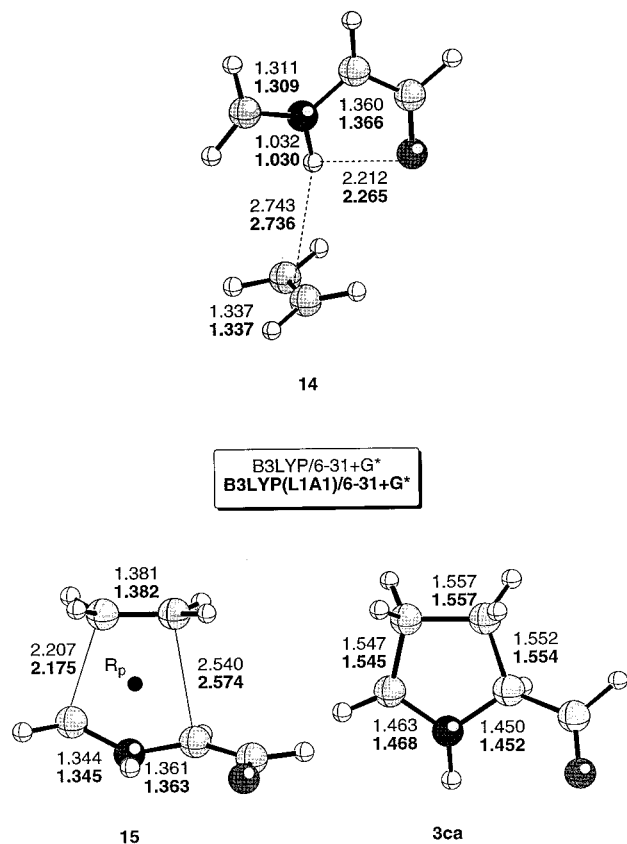


Figure 7. Main geometric features of the stationary points found in the $1c + 2a \rightarrow 3ca$ reaction (Scheme 8). See the captions of Figures 1 and 2.

Scheme 8

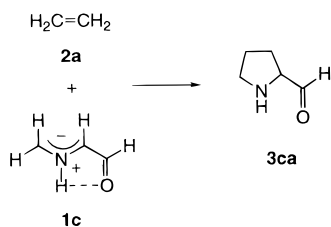


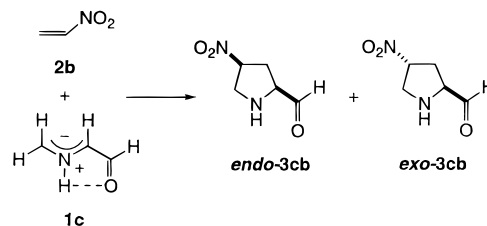
Table 4. Complexation Energies^a (ΔE_c , kcal/mol), Activation Energies^b (ΔE_a , kcal/mol), and Reaction Energies^c (ΔE_{rxn} , kcal/mol) of the $1c + 2a \rightarrow 3ca$ Reaction^d (see Scheme 8)

method	ΔE_c	ΔE_a	ΔE_{rxn}
HF/6-31+G*	-1.9	26.2	-50.2
MP2/6-31+G* ^e	-4.0	7.2	-47.8
B3LYP/6-31+G*	-1.7	13.7	-33.1
B3LYP(L1A1)/6-31+G* ^f	+7.2	13.9	-26.0

^a Computed as $\Delta E_c = E(14) - [E(1c) + E(2a)]$. ^b Computed as $\Delta E_a = E(15) - E(14)$. ^c Computed as $\Delta E_{rxn} = E(3ca) - [E(1c) + E(2a)]$. ^d The zero-point energy corrections, conveniently scaled if necessary (see text) were computed at the geometry optimization level. ^e Single-point energy computed on the HF/6-31+G* optimized structures. ^f The energy differences in solution were computed in acetonitrile ($\epsilon = 35.94$).

points found in the B3LYP/6-31+G* energy hypersurfaces, both in the gas phase and in solution, are reported in Figure 7, and the corresponding energy differences are shown in Table 4. According to our results, the stability of the orientation complex **14** with respect to the reactants is quite low in the gas phase. When the complexation energy is computed in acetonitrile solution, inclusion of ZPVE results in a positive value (if the ZPVE correlation is not included, **14** lies 0.2 kcal/mol below

Scheme 9^a



^a In the chiral structures only one enantiomer is drawn.

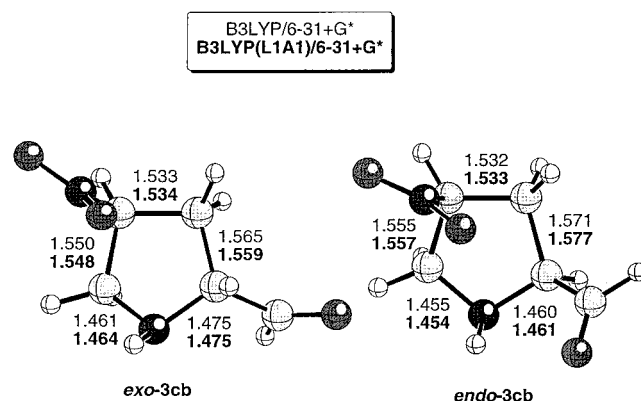
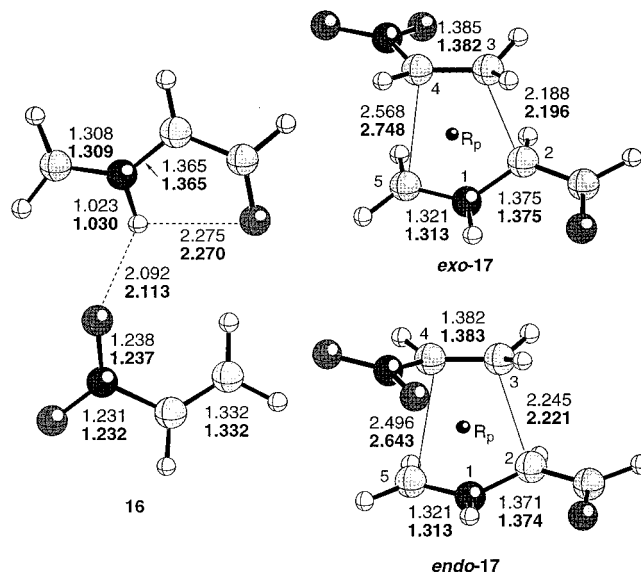


Figure 8. Chief geometric features of the stationary points found in the $1c + 2b \rightarrow 3cb$ reaction (Scheme 9). See the captions of Figures 1 and 2.

the separate reactants **1c** and **2a**). Therefore, although the computed ΔE_a values reported in Table 4 are quite similar in the gas phase and in solution, if the activation energy is estimated from the separate reagents, the energy barrier is significantly larger in solution.

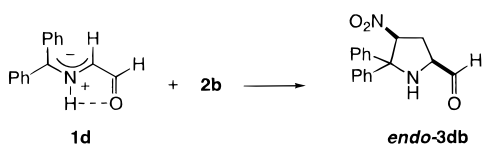
The structure of **15** is depicted in Figure 7. This transition structure is also concerted, with a computed synchronicity of 0.79 in the gas phase. In addition, the computed NICS at the (3,+1) ring point is -21.30 ppm, which is an indicator of an aromatic transition structure.

Then we studied computationally the interaction between azomethine ylide **1c** in its **A** conformation and nitroethylene **2b**. In this case, two diastereomers can be formed, *endo*-**3cb** and *exo*-**3cb** (Scheme 9). The stationary points located in the gas phase and in solution are shown in Figure 8, and the main

Table 5. Complexation Energies^{a,b} (ΔE_c , kcal/mol), Activation Energies^{a,c} (ΔE_a , kcal/mol), Reaction Energies^{a,d} (ΔE_{rxn} , kcal/mol), Synchronicities^a (S_y), NICS^e (ppm/mol), and TS-Dipole Moments^a (μ_{TS} , au) of **1c** + **2b** \rightarrow **3cb** Reaction

magnitude	1c + 2b \rightarrow <i>endo</i> - 3cb		1c + 2b \rightarrow <i>exo</i> - 3cb	
	$\epsilon = 1.00$	$\epsilon = 35.94$	$\epsilon = 1.00$	$\epsilon = 35.94$
ΔE_c	-7.3	+6.6	-7.3	+6.6
ΔE_a	5.8	14.4	5.2	17.3
ΔE_{rxn}	-35.1	-24.0	-35.4	-22.2
S_y	0.78	0.63	0.76	0.61
NICS	-19.98	-18.44	-18.44	-15.86
μ_{TS}	2.54	3.40	1.33	2.12

^a Computed at the B3LYP/6-31+G* + Δ ZPVE and the B3LYP-(L1A1)/6-31+G* + Δ ZPVE levels in the gas phase and in solution, respectively. ^b Computed as $\Delta E_c = E(\mathbf{16}) - [E(\mathbf{1c}) + E(\mathbf{2b})]$. ^c Computed as $\Delta E_a = E(\mathbf{17}) - [E(\mathbf{1c}) + E(\mathbf{2b})]$. ^d Computed as $\Delta E_{\text{rxn}} = E(\mathbf{3cb}) - [E(\mathbf{1c}) + E(\mathbf{2b})]$. ^e Computed at the GIAO-SCF/6-31+G**//B3LYP/6-31+G* and the GIAO-SCF/6-31+G**//B3LYP(L1A1)/6-31+G* levels in the gas phase and in solution, respectively.

Scheme 10^a

^a In *endo*-**3db** only one enantiomer is drawn.

energetic and electronic features of the whole process are reported in Table 5.

The shape of **16** resembles that found for **8** since the interaction between the azomethine ylide and the alkene takes place through one oxygen atom of the nitro group. However, the energy of complexation is again positive in solution when the ZPVE is taken into account (Table 5). Without this correction **16** lies 0.92 kcal/mol below the separate reactants at the B3LYP(L1A1)/6-31+G* in acetonitrile solution. Therefore, we can conclude that this complex is not chemically relevant under the usual experimental conditions.

We have located two diastereomeric transition structures, *exo*-**17** and *endo*-**17**, that correspond to *supra*-*supra* concerted mechanisms. It is interesting to note that if solvent effects are considered, formation of *endo*-**3cb** is favored under both kinetic and thermodynamic control (see Table 5). In addition, *endo*-**17** is more aromatic and more synchronous than its *exo* analogue. As can be seen from the geometric data reported in Figure 8, these transition structures are quite asynchronous, particularly in solution. Thus, the calculated synchronicities are found to be ~ 0.6 for both process, the *exo*-pathway being slightly more asynchronous (See Table 5). Therefore, both transition structures correspond to almost "halfway" process in terms of synchronicity. This feature is readily appreciated if we examine the evolution of the C2 \cdots C3 and C4 \cdots C5 bond distances on passing from *endo*- and *exo*-**17** to *endo*- and *exo*-**3cb**. In Figure S3 of the Supporting Information we have included the plot of these distances against the intrinsic reaction coordinate (IRC). From these data it can readily be seen that at IRC ≈ 1.2 au the C2-C3 bond is already formed, whereas the C4 \cdots C5 distance is still larger than 2 Å. Therefore, we conclude that this example is a limiting case between a concerted and a stepwise mechanism. Inclusion of adequate substituents at the 1,3-dipole could result in stepwise processes.

To confirm this hypothesis, we have studied the reaction between nitroethylene **2b** and azomethine ylide **1d** to form compound *endo*-**3db** (Scheme 10). As we had previously found in the metalated version of the reaction, we expected that

inclusion of two phenyl groups in the starting azomethine could stabilize the corresponding zwitterionic intermediates. Given the size of the system, the search of the stationary points and the geometric optimizations were performed on the HF/3-21G and HF(L1A1)/3-21G energy hypersurfaces. The lowest energy conformations of several structures were located by Monte Carlo simulations using the AMBER* force field. The single point energies were then computed both in the gas phase and in acetonitrile solution at the B3LYP/6-31+G* and B3LYP(L1A1)/6-31+G* levels, respectively. The reaction profiles thus characterized are depicted in Figure 9.

We have found that under the substituent effect the reaction turns out to be stepwise. The first transition structure, **18** is associated with the formation of the C2 \cdots C3 bond, the corresponding distance being 2.272 Å in acetonitrile solution. The calculated C4-C5 distance is 3.253 Å in solution, which is an indicator of no appreciable bonding interaction between these atoms. We have also located a zwitterionic intermediate **19** in which the C2-C3 bond is completely formed and there is an intramolecular hydrogen bond between the O7 atom and the hydrogen atom bonded to N1. It is interesting to note that this intermediate was located only in solution, since in the gas phase the optimized structure has the hydrogen atom bonded to O7, i.e., the nitro group is in its *aci* form (Figure 9).

The nitro tautomer of the latter structure, denoted as **22** in Figure 9 lies ~ 25 kcal/mol below *endo*-**19** in the gas phase. Another isomer of this zwitterionic intermediate is **20**, which possesses an O7-C5 bond and is slightly more stable than *endo*-**19** in solution (see Figure 9). This structure resembles those experimentally found by Mayr et al. during their studies on [4 + 3] cycloadditions between 1,3-dipoles and dienes.⁵¹ Finally, we found the second transition structure *endo*-**21**, in which C4 \cdots C5 is found to be 2.439 Å in acetonitrile solution. An IRC calculation in acetonitrile solution showed that this saddle point connects the cycloadduct *endo*-**3db** with **20**.

We performed several series of experiments to test the main predictions made by our computations on model compounds. First, we studied the variation of the reaction rate of the **1b** + **2c** \rightarrow **3bc** process with the solvent. As in the metal-assisted version of the reaction, only the *endo* cycloadduct was obtained. We measured these reaction rates by monitoring the decay of the $\pi \rightarrow \pi^*$ UV absorption of the starting nitroalkenes (Figure S4 of the Supporting Information). Since the measurement of the required absorbance was difficult at large reaction times, we used the Kezdy-Swinbourne method to determine the A_{∞} values.⁵² The plots used for the determination of A_{∞} and k_{obs} in toluene solution are also shown in Figure S4. The observed kinetic constants are reported in Table 6 and show an acceleration of the reaction with increasing polarity of the solvent. The corresponding logarithmic values against the Onsager function $(\epsilon - 1)/(2\epsilon + 1)$ are shown in Figure S5. These experimental findings are in line with the computed solvent dependence of the formation of azomethine ylide **1c** from the enol derivative **1'c** via **13**. In contrast, Huisgen et al.⁵³ found that in solvents of increasing polarity [3 + 2] dipolar cycloadditions between alkenes and nitrones exhibit a moderate rate deceleration.

(51) Mayr, H.; Baran, J.; Heigl, U. W. *Gazz. Chim. Ital.* **1991**, *121*, 373.

(52) Espenson, J. H. *Chemical Kinetics and Reaction Mechanisms*; McGraw-Hill: New York, 1981; pp 24-27.

(53) Geittner, J.; Huisgen, R.; Reissig, H.-V. *Heterocycles* **1978**, *11*, 109. (b) Huisgen, R.; Seidl, H.; Brüning, I. *Chem. Ber.* **1969**, *102*, 1102. (c) Eckell, A.; George, M. V.; Huisgen, R.; Kende, A. S. *Chem. Ber.* **1977**, *110*, 578. See also: Böhm, T.; Elender, K.; Riebel, P.; Troll, T.; Weber, A.; Sauer, J. *Tetrahedron* **1999**, *55*, 9515.

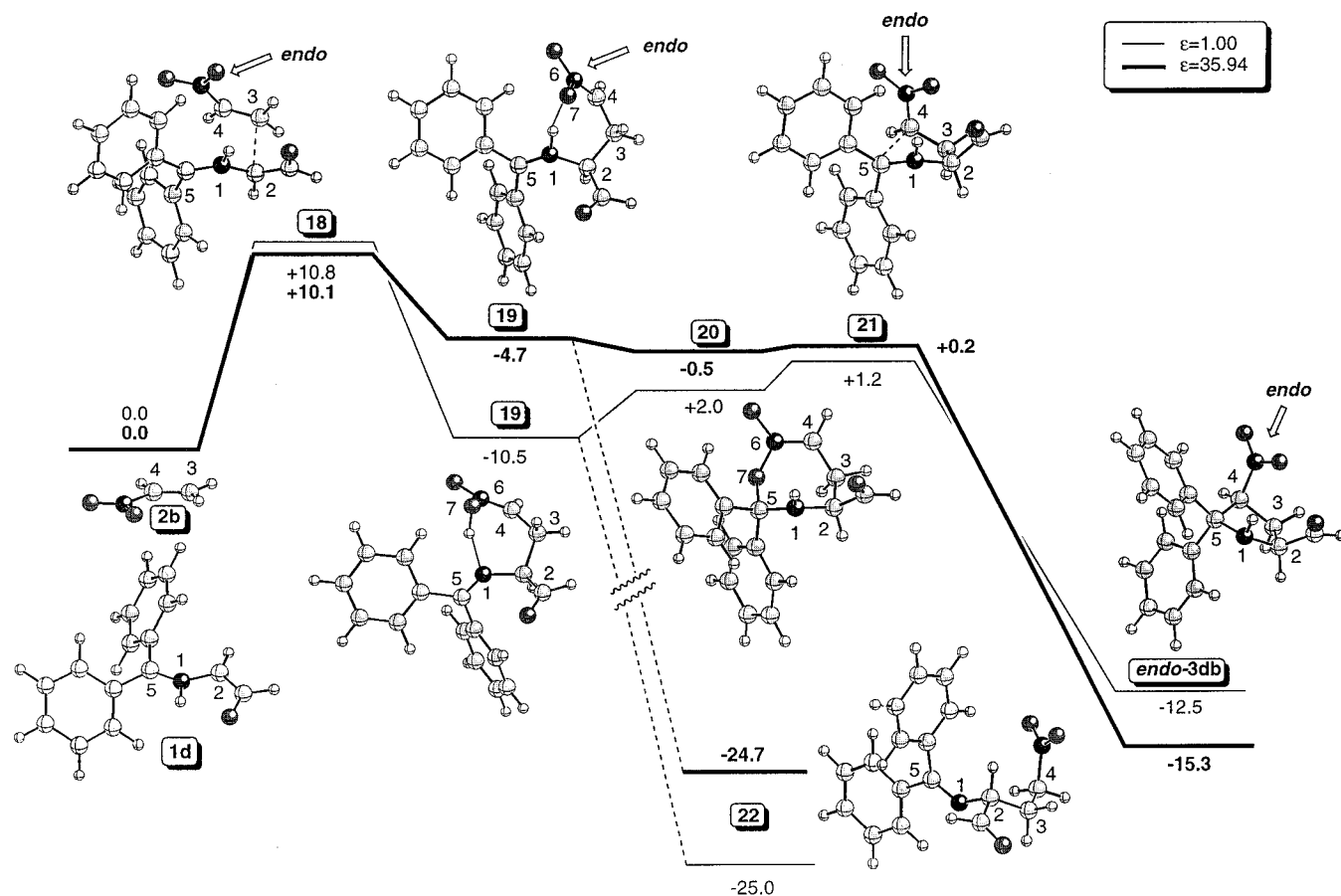


Figure 9. Reaction profiles found in vacuo and in acetonitrile solution ($\epsilon = 35.94$) for the **1d** + **2b** \rightarrow **3db** reaction (Scheme 10). See the captions of Figures 1 and 2.

Table 6. Observed First-Order Rate Constants $k_{\text{obs}}^{a,b}$ for the **1b** + **2c** \rightarrow **3bc** Reaction in Different Solvents

solvent	$(\epsilon - 1)/(2\epsilon + 1)^c$	$10^4 k_{\text{obs}}$ (s^{-1})	$-\ln k_{\text{obs}}$
$\text{C}_6\text{H}_5\text{CH}_3$	0.24	0.69 (± 0.03)	9.58
$\text{C}_6\text{H}_5\text{Br}$	0.37	1.21 (± 0.05)	9.02
<i>o</i> - $\text{C}_6\text{H}_4\text{Cl}_2$	0.43	1.77 (± 0.12)	8.64
$\text{C}_6\text{H}_5\text{CN}$	0.47	1.75 (± 0.13)	8.65

^a Computed by means of the Kezdy–Swinbourne method (see text).

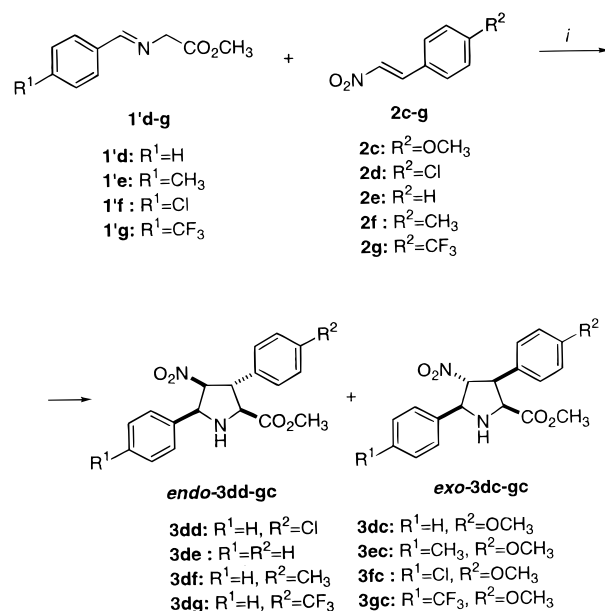
^b Kinetic measurements were carried out at 112 °C in a 0.02 M solution of the nitroalkene **2c** and with an excess of 10 equiv of **1b**. ^c Onsager function where ϵ stands for the dielectric constant of the solvent.

Therefore, our results indicate that formation of the dipole is a relevant step in the thermal [3 + 2] cycloaddition between imines and π -deficient alkenes.

In addition, we have detected by ^1H NMR the formation of **4bc** in the reaction between **1b** and **2c** to form *endo*-**3bc**, as we did in the metalated version of this reaction. The structure of **4bc** was unambiguously determined by transformation to its acetamide **5bc** (vide supra). Thus, after 20 and 46 h in refluxing toluene the *endo*-**3bc**:**4bc** ratios were 83:17 and 67:33, respectively. This is in agreement with our computational results on the stepwise nature of this reaction and on the relative energies of *endo*-**3db** and **22**. In addition, these results indicate that the conversion from **19** to **22** (not included in our computational study) has a larger activation barrier than the **19** \rightarrow **3db** transformation.

We have also studied the thermal reaction between imines **1d–g** and nitroalkenes **2c–g** to yield the cycloadducts depicted in Scheme 11. In these cases, almost equimolar amounts of *endo*- and *exo*-cycloadducts were obtained. The structures of these cycloadducts were unequivocally assigned by comparison

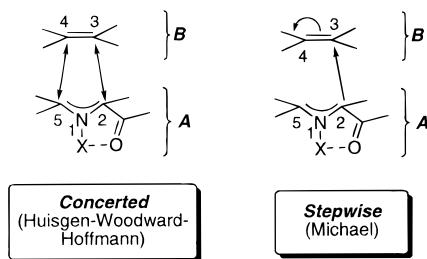
Scheme 11^a



^a In the chiral compounds only one enantiomer is drawn. ^b Reagents and conditions: i: Toluene, 112 °C.

with structurally related compounds.¹⁶ In addition, we have not detected Michael cycloadducts in these reactions. This result suggests that these less substituted azomethine ylides react via mechanisms closer to that described in the study on the **1c** + **2b** \rightarrow **2cb** reaction (Scheme 9), the relative energies of the corresponding *endo*- and *exo* transition states being quite similar.

Scheme 12



Origins of the Concerted and Stepwise Mechanisms. In the previous sections we have found that different mechanisms can operate in a similar transformation and that the stereochemical criterion is not always a useful indicator of the nature of the mechanism. In principle, there are two limiting mechanisms for the [3 + 2] cycloaddition between azomethine ylides and alkenes. In the concerted mechanism, there are bonding interactions between the C2 and C3 atoms, as well as between C4 and C5 (Scheme 12). From second-order perturbation theory,⁵⁴ the following expression is obtained for the initial stages of the concerted process:

$$\Delta E_{\text{con}} = \Delta E_{\text{orb}}^{A \rightarrow B} + \Delta E_{\text{orb}}^{B \rightarrow A} = 2 \frac{(c_2^{\text{H}} c_3^{\text{L}} \beta_{23} + c_5^{\text{H}} c_4^{\text{L}} \beta_{45})^2}{\epsilon_{\text{A}}^{\text{H}} - \epsilon_{\text{B}}^{\text{L}}} + 2 \frac{(c_2^{\text{L}} c_3^{\text{H}} \beta_{23} + c_5^{\text{L}} c_4^{\text{H}} \beta_{45})^2}{\epsilon_{\text{B}}^{\text{H}} - \epsilon_{\text{A}}^{\text{L}}} \quad (1)$$

where c_i^{H} and c_i^{L} are the expansion coefficients of HOMO and LUMO at the i -atom, respectively. Similarly, $\epsilon_{\text{k}}^{\text{H}}$ and $\epsilon_{\text{k}}^{\text{L}}$ are the HOMO and LUMO energies of the k -species, (**A** or **B**, see Scheme 12), respectively. The β_{ij} terms in eq 1 are the resonance integrals between the AOs of the i - and j -atoms.

If we consider a stepwise reaction, the first step consists of a nucleophilic attack of azomethine **A** on the alkene **B**. In other words, the stepwise mechanism is initiated by a conjugate (Michael) addition of an enolate on an electrophilic alkene (Scheme 12). In this case, the nucleophilic addition can be described in its initial stages as the result of a combined electrostatic and orbital stabilizing interaction according to the following equation:

$$\Delta E_{\text{Nu}} = \Delta E_{\text{Coul}} + \Delta E_{\text{orb}}^{\text{Nu}} = \sum_{i \in \text{B}} \frac{q_2 q_i}{R_{2i}} + 2 \frac{(c_2^{\text{H}} c_3^{\text{L}} \beta_{23})^2}{\epsilon_{\text{A}}^{\text{H}} - \epsilon_{\text{B}}^{\text{L}}} \quad (2)$$

where q_2 and q_i are the charges of the C2 and i atoms, and R_{2i} is the distance between C2 and the i -atom.

In addition to these stabilizing interactions, there is a repulsive term which is responsible for the positive slope of the potential energy versus reaction coordinate from the reactants to the transition structure. At the initial stages of the reaction this repulsive term can be approximated as⁵⁴

$$\Delta E_{\text{rep}} = -2(\beta_{23} S_{23} + \beta_{45} S_{45}) \quad (3)$$

where β_{ij} and S_{ij} are the resonance and overlap integrals between the i - and j -atoms, respectively. Since for both the concerted and stepwise mechanisms the ΔE_{rep} terms are similar, the nature of the mechanism is determined mainly by the alternative interactions described by eqs 1 and 2. Therefore, the condition

(54) (a) Salem, L. *J. Am. Chem. Soc.* **1968**, *90*, 543. (b) Salem, L. *J. Am. Chem. Soc.* **1968**, *90*, 223.

Table 7. Intrinsic Reaction Coordinate Values (IRC au),^a

Internuclear Distances (R_{ij} , Å),^b Overlap Integrals (S_{ij} , au),^c Repulsive Energies (ΔE_{rep} , kcal/mol),^d Michael Energies (ΔE_{Nu} , kcal/mol),^e and Huisgen–Woodward–Hoffmann Energies (ΔE_{con} , kcal/mol)^f for Selected Model [3 + 2] Reactions

IRC	R_{23}	S_{23}	R_{45}	S_{45}	ΔE_{rep}	ΔE_{Nu}	ΔE_{con}	$\Delta E_{\text{orb}}^{\text{Nu}} \Delta E_{\text{con}}$
1c + 2a → 3ca								
−3.978	3.511	0.017	3.578	0.014	0.19	0.03	−0.05	0.30
−2.994	3.290	0.026	3.301	0.025	0.51	0.05	−0.13	0.27
−1.897	3.055	0.041	2.984	0.047	1.49	0.07	−0.38	0.23
−0.897	2.797	0.066	2.684	0.080	4.13	0.10	−1.06	0.22
1c + 2b → endo-3cb								
−3.932	3.455	0.019	3.654	0.012	0.19	−1.52	−0.11	0.43
−2.988	3.248	0.028	3.457	0.018	0.45	−1.77	−0.25	0.43
−1.894	2.979	0.047	3.190	0.032	1.27	−2.03	−0.72	0.43
−0.896	2.677	0.081	2.941	0.051	3.60	−2.35	−2.04	0.45
1a + 2b → endo-3ab								
−3.960	3.469	0.018	3.833	0.008	0.15	−1.30	−0.06	0.71
−2.986	3.272	0.027	3.636	0.013	0.34	−1.54	−0.13	0.71
−1.894	3.029	0.043	3.448	0.019	0.85	−1.83	−0.32	0.73
−0.986	2.730	0.074	3.314	0.025	2.38	−2.25	−0.90	0.78

^a Computed at the HF/6-31G* level. ^b See Scheme 13 for the numbering system. ^c Computed by means of eq 6. ^d Computed by means of eq 3. ^e Computed by means of eq 2. ^f Computed by means of eq 1.

for concertedness is

$$[\Delta E_{\text{orb}}^{A \rightarrow B} - \Delta E_{\text{orb}}^{\text{Nu}}] + \Delta E_{\text{orb}}^{B \rightarrow A} > \Delta E_{\text{Coul}} \quad (4)$$

To evaluate quantitatively eqs 1–4, several additional approximations are required. First, we have computed the resonance integrals β_{ij} by means of the Mulliken approximation:⁵⁵

$$\beta_{ij} \approx \frac{1}{2}(\beta_i^{\circ} + \beta_j^{\circ}) S_{ij} \quad (5)$$

where S_{ij} is the corresponding overlap integral and β_i° and β_j° are fixed parameters for the i - and j -atoms, respectively.⁵⁶ The overlap integrals can be evaluated from the analytical formulas reported by Mulliken⁵⁷ for overlapping Slater-type orbitals (STOs). For σ -overlap between two 2p AOs of carbon, the analytical expression is

$$S_{ij} = \left[-1 - \xi R_{ij} - \frac{\xi^2 R_{ij}^2}{5} + 2 \frac{\xi^3 R_{ij}^3}{15} + \frac{\xi^4 R_{ij}^4}{15} \right] \exp(\xi R_{ij}) \quad (6)$$

where R_{ij} is the internuclear distance between i and j and ξ is the Slater exponent. The parameters⁵⁶ used in our quantitative evaluation of expressions 5 and 6 are $\beta_i^{\text{pp}} = \beta_j^{\text{pp}} = -0.28367$ hartree and $\xi = 1.685$ bohr^{−1} (See Figure S6 of the Supporting Information for additional details). The charges required for the evaluation of ΔE_{Coul} have been computed using the NBO charges at the different atoms of the separate reagents. Finally, the R_{ij} values were obtained from IRC studies performed on selected reactions at the HF/6-31G* level.

We have selected the **1c** + **2a** → **3ca** and **1a** + **2b** → *endo*-**3ab** reactions as model examples for concerted and stepwise mechanisms respectively, and the **1c** + **2b** → *endo*-**3cb** transformation as an example of a limiting case between both mechanisms (*vide supra*).

The computed ΔE_{rep} , ΔE_{Nu} , and ΔE_{con} energies at different points are reported in Table 7. From these data, it is clear that

(55) (a) Mulliken, R. S. *J. Chem. Phys.* **1949**, *46*, 675. (b) Mulliken, R. S. *J. Chem. Phys.* **1952**, *56*, 295.

(56) Dewar, M. J. S.; Zoebisch, E. G.; Healy, E. F.; Stewart, J. J. P. *J. Am. Chem. Soc.* **1985**, *107*, 3902.

(57) Mulliken, R. S.; Rieke, C. A.; Orloff, D.; Orloff, H. *J. Chem. Phys.* **1949**, *17*, 1248.

in the $1c + 2a \rightarrow 3ca$ reaction the concerted mechanism is largely preferred, since the ΔE_{Nu} terms are indeed repulsive at the first stages of the interaction. In the case of the $1c + 2b \rightarrow endo-3cb$ reaction, the nucleophilic term becomes more significant as long as the reaction progresses. In addition, the ΔE_{orb}^{Nu} is near 50% of the ΔE_{con} term, thus indicating that this is a limiting case, and that substituent and/or solvent effects can modify the mechanism from concerted to stepwise. Finally, in the case of the $1a + 2b \rightarrow endo-3ab$ reaction the stepwise mechanism is clearly preferred, and ΔE_{orb}^{Nu} is almost 75% of ΔE_{con} . In the latter cases the nitro group induces a significant polarization in the nitroalkene thus enhancing its electrophilicity. This promotes an asymmetric transfer of electron density from the azomethine to the dipolarophile. From eqs 1 and 2 we readily appreciate that if c_3^L and c_2^H are large and the difference of energy between the HOMO of the nitroalkene and the LUMO of the azomethine ylide increases, then ΔE_{con} is close to ΔE_{orb}^{Nu} (see Table 8), thus favoring the stepwise mechanism, especially if electrostatic interactions (and eventually the electrostatic contribution of the solvation energy) are adequate.

Conclusions

From the combined theoretical and experimental studies reported in this paper the following conclusions can be drawn:

(a) The interaction between *N*-metalated azomethine ylides and nitroalkenes as representative π -deficient olefins is stepwise, the first step being a conjugate nucleophilic addition in which the azomethine ylide acts as an enolate and the nitroalkene behaves as a Michael acceptor. Under favorable conditions, the corresponding zwitterionic intermediate can be trapped and its transformation into the [3 + 2] cycloadduct observed.

(b) The reaction between *N*-unsubstituted azomethine ylides and nitroalkenes can be concerted or stepwise, depending upon the nature of the substituents.

(c) The concerted or stepwise nature of the alternative reaction mechanisms can be understood and predicted using second-order perturbation theory. Since eq 4 is general for any thermal cycloaddition and approximations 5 and 6 are also quite general, the analysis can be extended to other thermal cycloadditions. Thus, within the limitations previously discussed, the nature of the mechanism can be anticipated from eqs 1 and 2, using internuclear distances of ~ 3.0 Å.

Experimental Section

General. Commercially available compounds were used as purchased without further purification. LiClO₄ (ACS reagent) was used as received (CAUTION: perchlorates are potentially explosive materials. Under the experimental conditions described below, this compound can be used safely). All solvents were dried and distilled according to standard protocols.⁵⁸ Nitroalkenes **2c–g** were prepared following reported procedures.⁵⁹ Imines **1d–g** and **1c** were prepared as previously reported by us¹⁶ and by O'Donnell,⁶⁰ respectively. Cycloadducts **3dd** and **3dc** were characterized by comparison with the previously reported data.¹⁶ Chemical shifts in the ¹H NMR and ¹³C NMR spectra are reported as δ values (ppm) with respect to TMS and in deuterated chloroform. Flash chromatography purifications were performed using silica gel 60–230 mesh and AcOEt/hexanes mixtures varying from 1:10 to 1:20. After the corresponding extractions, the organic layers were dried with Na₂SO₄ prior to evaporation of the solvent under reduced pressure.

(58) Perrin, D. D.; Armarego, N. L. F. *Purification of Laboratory Chemicals*; Pergamon: Oxford, 1993.

(59) Bourguignon, J.; LeNard, G.; Gueguiner, G. *Can. J. Chem.* **1985**, *63*, 2354.

(60) O'Donnell, M. J.; Polt, R. L. *J. Org. Chem.* **1982**, *47*, 2663.

General Procedures for the Reaction of the Imines 1' and the Nitroalkenes 2. Method A. The imine **1'** (5 mmol) was dissolved in CH₃CN (25 mL), and then NEt₃ (0.7 mL, 5 mmol), the nitroalkene **2** (5 mmol) and LiClO₄ (0.53 g, 5 mmol) were added. The progress of the reaction was monitored by TLC. After completion of the reaction, the mixture was washed with saturated aqueous NH₄Cl solution (2 × 10 mL) and water (4 × 5 mL). After evaporation, the crude mixture was triturated in Et₂O, and the precipitated cycloadduct was recrystallized in Et₂O–hexanes.

Method B. A mixture of the imine **1'** (5 mmol) and the nitroalkene **2** (5 mmol) in the appropriate solvent (25 mL) was heated at 112 °C for 24 h. After completion of the reaction, the solution was cooled and the solvent removed under reduced pressure. The different cycloadducts were separated from the reaction mixture by flash chromatography.

(2S*,3R*,4S*)-5,5-Diphenyl-2-methoxycarbonyl-3-(4-methoxyphenyl)-4-nitropyrrolidine (endo-3bc): following the method A: yield 1.73 g (80%); mp 137–139 °C; IR (KBr) 3307, 1752, 1551, 1344 cm⁻¹; ¹H NMR (δ ppm, CDCl₃, D₂O) 7.77–6.61 (m, 14H), 6.01 (d, 1H, *J* = 4.0 Hz), 4.06 (dd, 1H, *J* = 8.7 Hz, *J'* = 3.8 Hz), 3.96 (d, 1H, *J* = 8.8 Hz), 3.73 (s, 6H); ¹³C NMR (δ ppm, CDCl₃) 172.5, 159.8, 142.5, 129.9, 129.6, 129.3, 129.0, 128.6, 128.4, 127.4, 126.1, 114.9, 102.3, 77.9, 66.1, 58.6, 55.9, 53.2. Anal. Calcd for C₂₅H₂₄O₅N₂: C, 69.42; H, 5.60; N, 6.48. Found: C, 69.27; H, 5.63; N, 6.44.

(2S*,3R*)-Methyl 2-acetamido-3-(4-methoxyphenyl)-4-nitrobutyrate (5bc). Imine **1'b** (1.27 g, 5 mmol) was dissolved in CH₃CN (25 mL), and then NEt₃ (0.7 mL, 5 mmol), the nitroalkene **2c** (0.90 g, 5 mmol), and LiClO₄ (0.53 g, 5 mmol) were added. After 1 h of reaction at room temperature, a 25:75 mixture of *endo-3bc* and imine **4bc** was observed by ¹H NMR. The crude reaction mixture was treated according to the general procedure A, and the resulting oily residue was dissolved in THF (15 mL) and 2 N HCl (0.8 mL). The resulting mixture was stirred for 20 min at room temperature. Usual basic workup and evaporation of the solvent gave an oily residue which was diluted with CH₂Cl₂ (22 mL). To the resulting solution, trifluoroacetic acid (1.5 mL, 20 mmol) was added dropwise, and the resulting mixture was stirred at room temperature for 5 h. The volatiles were evaporated, and the resulting mixture was dissolved in CH₂Cl₂ (8 mL). This solution was treated with NEt₃ (0.42 mL, 3.12 mmol) and acetic anhydride (0.3 mL, 2.9 mmol) and stirred overnight at room temperature. The resulting mixture was washed with 1 N HCl (5 mL), NaHCO₃ (saturated solution, 5 mL) and water (5 mL). The organic layer was dried, and evaporation of the solvent gave a solid which was crystallized from AcOEt/hexanes. Yield: 0.403 g (26% from **1'b**); mp 146–147 °C; IR (KBr) 3308, 1742, 1660, 1554, 1252 cm⁻¹; ¹H NMR (δ ppm, CDCl₃) 7.10–6.82 (m, 4H), 6.15 (db, 1H, *J* = 8.5 Hz), 4.87 (m, 3H), 3.86 (m, 1H), 3.78 (s, 3H), 3.57 (s, 3H), 2.03 (s, 3H); ¹³C NMR (δ ppm, CDCl₃) 170.4, 169.9, 159.6, 129.1, 126.4, 114.4, 77.1, 55.2, 54.8, 52.5, 46.3, 23.1. Anal. Calcd for C₁₄H₁₈O₆N₂: C, 54.18; H, 5.85; N, 9.03. Found: C, 53.92; H, 5.84; N, 8.98.

General Procedure for the Kinetic Measurements. In a round-bottomed flask sealed with a Liebig refrigerator the imine **1'** (5 mmol) and the nitroalkene **2** (0.5 mmol) were dissolved in the selected solvent (25 mL). The mixture was placed in an oil bath and under constant pressure. At certain time aliquots were withdrawn with a syringe, immediately quenched by cooling to 0 °C, diluted to a concentration of 10⁻⁴M, and analyzed by UV spectroscopy.

Given the nature of the UV spectra, the *A*_∞ values were calculated by means of the Kezdy–Swinbourne method.⁵² According to this procedure, the absorbances at *t* and *t* + τ times fulfill the following condition:

$$\frac{A_t - A_\infty}{A_{t+\tau} - A_\infty} = \exp(k_{obs}\tau) \quad (8)$$

Therefore,

$$A_t = A_\infty[1 - \exp(k_{obs}\tau)] + A_{t+\tau}\exp(k_{obs}\tau) \quad (9)$$

Since the first term of eq 9 is time-independent, a plot of *A*_{*t*} versus *A*_{*t*+ τ} will be linear with a slope of $\exp(k_{obs}\tau)$. At the end point, *A*_{*t*} = *A*_{*t*+ τ} = *A*_∞. Therefore, the intersection of the line through the data points

with the 45° line gives the value of A_{∞} . We have used τ values of $\sim 1/2$, as recommended,⁵² to provide greatest accuracy. Finally, the k_{obs} values were determined in the usual way by means of linear regressions, as shown in Figure S4 of the Supporting Information.

(2S*,3R*,4S*)-3-(4-Chlorophenyl)-2-Methoxycarbonyl-4-nitro-5,5-diphenylpyrrolidine (endo-3bd): following the method A: yield 1.64 g (82%); mp 164–165 °C; IR (KBr) 3309, 1741, 1545, 1547, 1341 cm⁻¹; ¹H NMR (δ ppm, CDCl₃) 7.77–6.65 (m, 14H, arom), 6.01 (d, 1H, $J = 4$ Hz), 4.08 (dd, 1H, $J = 9.0$ Hz, $J' = 4$ Hz), 3.98 (d, 1H, $J = 9.1$ Hz), 3.74 (s, 3H). ¹³C NMR (δ ppm, CDCl₃) 171.5, 141.9, 141.5, 135.8, 133.8, 129.2, 129.1, 129.0, 128.6, 128.0, 127.8, 126.6, 125.3, 101.2, 77.4, 65.3, 57.6, 52.6. Anal. Calcd for C₂₄H₂₁O₄N₂Cl: C, 65.97; H, 4.85; N, 6.41. Found: C, 65.42; H, 4.89; N, 6.42.

For the cycloadducts **3de**, **3df**, **3dg**, **3dc**, **3ec**, **3fc**, **3gc** the general procedure B in toluene was followed and a mixture of compounds *endo*- and *exo*- was obtained.

The cycloadducts *exo*-**3dg**, *endo*- and *exo*-**3fc**, *endo*-**3gc** were fully characterized as their *N*-acyl derivatives.

General Procedure for Obtaining the *N*-Acyl Derivatives. The corresponding cycloadduct (5 mmol) was dissolved in CH₂Cl₂ (50 mL), treated with TFA (50 mmol), and stirred at room temperature for 5 h. The volatiles were evaporated, and the product of the reaction dissolved in CH₂Cl₂ (45 mL). This solution was treated with NEt₃ (7 mmol) and acetic anhydride (6.5 mmol) and stirred for 48 h at room temperature. Then it was washed with HCl 1 N (12.5 mL), saturated aqueous NaHCO₃ solution (12.5 mL), and water (12.5 mL). The organic layer was dried with Na₂SO₄ and evaporated under reduced pressure, and the resulting syrup triturated in Et₂O yielding the acetylated compound.

(2S*,3R*,4S*,5S*)-2-Methoxycarbonyl-4-nitro-3,5-diphenylpyrrolidine (endo-3de): yield 0.343 g (21%); mp 120–122 °C; IR (KBr) 3314, 1735, 1545, 1370 cm⁻¹; ¹H NMR (δ ppm, CDCl₃) 7.44–7.25 (m, 10H), 5.27 (dd, 1H, $J = 6.5$ Hz, $J' = 3.2$ Hz), 4.91 (db, 1H, $J = 6.6$ Hz), 4.21 (dd, 1H, $J = 7.3$ Hz, $J' = 3.1$ Hz), 4.14 (d, 1H, $J = 7.4$ Hz), 3.80 (s, 3H), 3.35 (sb, 1H); ¹³C NMR (δ ppm, CDCl₃) 171.7, 138.5, 134.4, 129.2, 128.7, 128.0, 127.4, 126.4, 96.9, 67.7, 67.3, 55.3, 52.6. Anal. Calcd for C₁₈H₁₈O₄N₂: C, 66.24; H, 5.57; N, 8.58. Found: C, 66.05; H, 5.46; N, 8.58.

(2S*,3S*,4R*,5S*)-2-Methoxycarbonyl-4-nitro-3,5-diphenylpyrrolidine (exo-3de): yield 0.669 g (41%); mp 113–115 °C; IR (KBr) 3355, 1743, 1544, 1347 cm⁻¹; ¹H NMR (δ ppm, CDCl₃) 7.58–7.20 (m, 10H), 5.21 (t, 1H, $J = 8.0$ Hz), 4.75 (db, 1H, $J = 8.2$ Hz), 4.50 (d, 1H, $J = 9.0$ Hz), 4.37 (t, 1H, $J = 7.7$ Hz), 3.27 (s, 3H), 2.73 (sb, 1H); ¹³C NMR (δ ppm, CDCl₃) 171.8, 137.6, 135.8, 129.0, 128.9, 128.7, 128.1, 127.8, 126.8, 95.0, 67.6, 64.2, 53.7, 51.8. Anal. Calcd for C₁₈H₁₈O₄N₂: C, 66.24; H, 5.57; N, 8.58. Found: C, 65.70; H, 5.56; N, 8.58.

(2S*,3R*,4S*,5S*)-2-Methoxycarbonyl-3-(4-methoxyphenyl)-4-nitro-5-phenylpyrrolidine (endo-3df): yield 0.289 g (17%); mp 99–102 °C; IR (KBr) 3317, 1738, 1545, 1373 cm⁻¹. ¹H NMR (δ ppm, CDCl₃) 7.38–7.14 (m, 9H), 5.24 (dd, 1H, $J = 6.4$ Hz, $J' = 3.1$ Hz), 4.89 (db, 1H, $J = 6.0$ Hz), 4.16 (dd, 1H, $J = 7.4$ Hz, $J' = 3.0$ Hz), 4.11 (d, 1H, $J = 7.4$ Hz), 3.79 (s, 3H), 3.34 (sb, 1H), 2.35 (s, 3H); ¹³C NMR (δ ppm, CDCl₃) 171.7, 137.8, 135.5, 134.4, 129.9, 128.6, 127.3, 126.4, 97.0, 67.6, 67.3, 55.0, 52.5, 21.0. Anal. Calcd for C₁₉H₂₀O₄N₂: C, 67.03; H, 5.93; N, 8.23. Found: C, 66.80; H, 5.90; N, 8.15.

(2S*,3S*,4R*,5S*)-2-Methoxycarbonyl-3-(4-methylphenyl)-4-nitro-5-phenylpyrrolidine (exo-3df): yield 0.714 g (42%); mp 130–132 °C; IR (KBr) 3367, 1738, 1549, 1365 cm⁻¹; ¹H NMR (δ ppm, CDCl₃) 7.59–7.10 (m, 9H), 5.18 (t, 1H, $J = 8.0$ Hz), 4.74 (d, 1H, $J = 8.3$ Hz), 4.47 (d, 1H, $J = 9.0$ Hz), 4.33 (t, 1H, $J = 8.3$ Hz), 3.30 (s, 3H), 2.71 (sb, 1H), 2.29 (s, 3H); ¹³C NMR (δ ppm, CDCl₃) 172.0, 137.9, 137.7, 132.7, 129.4, 129.0, 128.9, 127.7, 126.9, 95.2, 67.6, 64.2, 53.5, 51.8, 21.0. Anal. Calcd for C₁₉H₂₀O₄N₂: C, 67.03; H, 5.93; N, 8.23. Found: C, 66.91; H, 5.85; N, 8.41.

(2S*,3R*,4S*,5S*)-3-Trifluoromethylphenyl-2-methoxycarbonyl-4-nitro-5-phenylpyrrolidine (endo-3dg): yield 0.394 g (20%); mp 155–157 °C; IR (KBr) 3353, 1736, 1555, 1321 cm⁻¹; ¹H NMR (δ ppm, CDCl₃) 7.69–7.25 (m, 9H), 5.27 (dd, 1H, $J = 6.7$ Hz, $J' = 4.0$ Hz), 4.92 (tb, 1H), 4.29 (dd, 1H, $J = 7.6$ Hz, $J' = 3.9$ Hz), 4.13 (tb, 1H), 3.81 (s, 3H), 3.30 (sb, 1H); ¹³C NMR (δ ppm, CDCl₃) 172.0, 143.0, 134.9, 129.7, 129.5, 128.8, 127.2, 127.0, 126.9, 97.2, 68.4, 67.9, 55.3,

53.5. Anal. Calcd for C₁₉H₁₇O₄N₂F₃: C, 57.86; H, 4.35; N, 7.10. Found: C, 57.55; H, 4.39; N, 7.10.

(2S*,3S*,4R*,5S*)-1-Acetyl-3-trifluoromethylphenyl-2-methoxycarbonyl-4-nitro-5-phenylpyrrolidine (acetyl derivative of *exo*-3dg): overall yield from **1'd** and **2g** 0.196 g (9%); mp 200–202 °C; IR (KBr) 1745, 1660, 1551, 1327 cm⁻¹; ¹H NMR (δ ppm, CDCl₃) 7.69–7.37 (m, 9H), 5.70 (dd, 1H, $J = 11.9$ Hz, $J' = 8.4$ Hz), 5.36 (d, 1H, $J = 8.5$ Hz), 5.16 (d, 1H, $J = 9.21$ Hz), 4.43 (t, 1H, $J = 10.7$ Hz), 3.36 (s, 3H), 1.68 (s, 3H); ¹³C NMR (δ ppm, CDCl₃) 170.7, 170.6, 137.6, 135.1, 129.7, 129.6, 128.3, 126.9, 126.0, 125.9, 125.8, 92.9, 66.7, 63.6, 52.2, 49.1, 22.7. Anal. Calcd for C₂₁H₁₉O₅N₂F₃: C, 57.80; H, 4.40; N, 6.42. Found: C, 57.60; H, 4.33; N, 6.42.

(2S*,3R*,4S*,5S*)-2-Methoxycarbonyl-3-(4-methoxyphenyl)-5-(4-methylphenyl)-4-nitropyrrrolidine (endo-3ec): yield 0.370 g (20%); mp 96–98 °C; IR (KBr) 3297, 1736, 1546, 1356 cm⁻¹; ¹H NMR (δ ppm, CDCl₃) 7.25–6.87 (m, 8H), 5.20 (dd, 1H, $J = 6.6$ Hz, $J' = 3.3$ Hz), 4.85 (db, 1H, $J = 6.1$ Hz), 4.14 (dd, 1H, $J = 7.3$ Hz, $J' = 3.3$ Hz), 4.08 (d, 1H, $J = 7.4$ Hz), 3.81 (s, 3H), 3.79 (s, 3H), 3.30 (sb, 1H), 2.32 (s, 3H); ¹³C NMR (δ ppm, CDCl₃) 171.9, 159.3, 138.5, 131.4, 130.6, 129.4, 128.6, 126.3, 114.6, 97.3, 67.6, 67.5, 55.3, 54.9, 52.6, 21.2. Anal. Calcd for C₂₀H₂₂O₅N₂: C, 64.84; H, 6.00; N, 7.56. Found: C, 64.45; H, 6.00; N, 7.62.

(2S*,3S*,4R*,5S*)-2-Methoxycarbonyl-3-(4-methoxyphenyl)-5-(4-methylphenyl)-4-nitropyrrrolidine (exo-3ec): yield 0.426 g (23%); mp 141–144 °C; IR (KBr) 3290, 1722, 1546, 1335 cm⁻¹; ¹H NMR (δ ppm, CDCl₃) 7.45–6.80 (m, 8H), 5.14 (t, 1H, $J = 8.1$ Hz), 4.68 (tb, 1H, $J = 8.1$ Hz), 4.43 (dd, 1H, $J = 9.1$ Hz, $J' = 5.4$ Hz), 4.31 (t, 1H, $J = 8.4$ Hz), 3.76 (s, 3H), 3.32 (s, 3H), 2.67 (tb, 1H), 2.36 (s, 3H); ¹³C NMR (δ ppm, CDCl₃) 172.0, 159.2, 138.6, 134.6, 129.6, 128.9, 127.6, 126.6, 114.0, 95.2, 67.3, 64.1, 55.1, 53.0, 51.8, 21.1. Anal. Calcd for C₂₀H₂₂O₅N₂: C, 64.84; H, 6.00; N, 7.56. Found: C, 64.54; H, 6.04; N, 7.56.

(2S*,3R*,4S*,5S*)-1-Acetyl-5-(4-chlorophenyl)-2-methoxycarbonyl-3-(4-methoxyphenyl)-4-nitropyrrrolidine (acetyl derivative of *endo*-3fc): overall yield from **1'f** and **2c** 0.173 g (8%); mp 220 °C; IR (KBr) 1747, 1657, 1551, 1398 cm⁻¹; ¹H NMR (δ ppm, CDCl₃) 7.68–6.83 (m, 8H), 5.56 (dd, 1H, $J = 11.9$ Hz, $J' = 8.5$ Hz), 5.31 (d, 1H, $J = 8.7$ Hz), 5.07 (d, 1H, $J = 9.4$ Hz), 4.29 (dd, 1H, $J = 11.9$ Hz, $J' = 9.5$ Hz), 3.77 (s, 3H), 3.40 (s, 3H), 1.67 (s, 3H); ¹³C NMR (δ ppm, CDCl₃) 171.8, 171.2, 160.6, 137.3, 130.5, 129.5, 129.0, 128.5, 123.0, 115.1, 94.2, 66.7, 64.5, 55.9, 52.9, 49.8, 23.4. Anal. Calcd for C₂₁H₂₁O₆N₂Cl: C, 58.26; H, 4.90; N, 6.47. Found: C, 57.94; H, 4.94; N, 6.45.

(2S*,3S*,4R*,5S*)-1-Acetyl-5-(4-chlorophenyl)-2-methoxycarbonyl-3-(4-methoxyphenyl)-4-nitropyrrrolidine (acetyl derivative of *exo*-3fc): overall yield from **1'f** and **2c** 0.184 g (8.5%); mp 214–215 °C; IR (KBr) 1742, 1661, 1556, 1393 cm⁻¹; ¹H NMR (δ ppm, CDCl₃) 7.68–6.83 (m, 8H), 5.56 (tb, 1H, $J = 8.6$ Hz), 5.31 (d, 1H, $J = 8.4$ Hz), 5.07 (d, 1H, $J = 9.4$ Hz), 4.29 (tb, 1H, $J = 10.1$ Hz), 3.78 (s, 3H), 3.40 (s, 3H), 1.67 (s, 3H); ¹³C NMR (δ ppm, CDCl₃) 171.9, 171.2, 160.6, 137.3, 130.5, 129.5, 129.0, 128.5, 123.0, 115.1, 94.2, 66.7, 64.5, 55.9, 52.9, 49.8, 23.4. Anal. Calcd for C₂₁H₂₁O₆N₂Cl: C, 58.26; H, 4.90; N, 6.47. Found: C, 57.95; H, 4.92; N, 6.38.

(2S*,3R*,4S*,5S*)-1-Acetyl-5-(4-trifluoromethylphenyl)-2-methoxycarbonyl-3-(4-methoxyphenyl)-4-nitropyrrrolidine (acetyl derivative of *endo*-3gc): overall yield from **1'g** and **2c** 0.222 g (9.5%); mp 200–204 °C; IR (KBr) 1742, 1661, 1554, 1326 cm⁻¹; ¹H NMR (δ ppm, CDCl₃) 7.98–6.84 (m, 8H), 5.55 (s, 1H), 5.12 (d, 1H, $J = 10.5$ Hz), 5.04 (d, 1H, $J = 6.1$ Hz), 3.95 (d, 1H, $J = 6.2$ Hz), 3.91 (d, 1H, $J = 6.4$ Hz), 3.78 (s, 3H), 3.72 (s, 3H), 1.92 (s, 3H); ¹³C NMR (δ ppm, CDCl₃) 171.8, 170.4, 160.0, 141.5, 128.8, 127.2, 126.7, 126.5, 121.8, 114.5, 95.9, 65.7, 62.2, 55.2, 52.8, 48.5, 21.9. Anal. Calcd for C₂₂H₂₁O₆N₂F₃: C, 56.65; H, 4.55; N, 6.00. Found: C, 56.50; H, 4.55; N, 6.05.

Acknowledgment. This work has been supported by the Gobierno Vasco-Eusko Jaurlaritza (Projects EX-1998-126 and PI-1998-116 and Fondo de Cooperación Aquitania/Euskadi/Navarra) and by the Provincial Government of Gipuzkoa (Gipuzkoako Foru Aldundia). We also thank Professor Carlos

Ubide (UPV/EHU) for helpful suggestions on the kinetic measurements.

Supporting Information Available: Tables of absolute energies and ZPVEs of all the stationary points discussed in the text and numerical data used in the elaboration of Figures

S1 and S2, Figures showing the evolution of the bond distances against IRC and variation of β against R (PDF). Crystallographic data for *endo*-**3bc** and **5bc** (CIF). This material is available free of charge via the Internet at <http://pubs.acs.org>.

JA9945360